A&A 455, 325–338 (2006)
DOI: 10.1051/0004-6361:20054598

Astronomy & Astrophysics

Dust in brown dwarfs

V. Growth and evaporation of dirty dust grains⋆

Ch. Helling[1] and P. Woitke[2]

[1] Astrophysics Missions Division, Research and Scientific Support Department ESTEC, ESA, PO Box 299, 2200 AG Noordwijk, The Netherlands
e-mail: chelling@rssd.esa.int
[2] Sterrewacht Leiden, PO Box 9513, 2300 RA Leiden, The Netherlands

Received 28 November 2005 / Accepted 28 April 2006

ABSTRACT

In this paper, we propose a kinetic description for the growth and evaporation of oxygen-rich, dirty dust particles, which consist of numerous small islands of different solid materials like Mg_2SiO_4, SiO_2, Al_2O_3, Fe and TiO_2. We assume that the total surface of such a grain collects condensible molecules from the gas phase and that these molecules are rapidly transported by diffusive hopping on the surface to the respective solid islands, where finally the constructive surface chemical reactions take place which increase the size of the grain. Applied to a typical dust forming region in a brown dwarf atmosphere, turbulent temperature fluctuations enable the creation of first seed particles (nucleation) at high supersaturation ratios. These seeds are then quickly covered by different solid materials in a simultaneous way, which results in dirty grains. Our treatment by moment equations allows for the calculation of the time-dependent material composition of the dust grains and the elemental composition of the gas phase. We argue that the depletion of condensible elements from the gas phase by dust formation may be incomplete and occurs in a patchy, non-uniform way which possibly makes metallicity measurements highly uncertain.

Key words. stars: atmospheres – stars: low-mass, brown dwarfs – methods: numerical – astrochemistry

1. Introduction

Dust is an essential part of brown dwarf atmospheres. It controls the opacity of the dust/gas mixture and influences the chemical, thermal and dynamical state of the atmosphere. Dust consumes condensible elements from the gas phase which weakens molecular absorption lines (Kirkpatrick et al. 1999; Burgasser et al. 2002; Geballe et al. 2002). Dust formation is a time-dependent process which may be the reason for non-periodic short-term variability (Bailer-Jones & Mund 1999, 2001a,b; Martín et al. 2001; Gelino et al. 2002; Maiti et al. 2005), recently also seen in polarisation measurements (Mènard et al. 2002; Maiti et al. 2005; Zapatero Osorio et al. 2005). Rockenfeller et al. (2006) point out evidence that more L dwarfs are non-periodically variable compared to M dwarfs. Spectro-polarimetry provides furthermore a possibility to measure the vertical distribution of the dust particles and their mean size in the atmosphere (Stam et al. 1999; Sengupta & Krishan 2001; Sengupta 2003; Sengputa & Kwok 2005; Stam & Hovenier 2005), if the refractory index of the dust grain material is known.

However, the actual material composition of the dust grains is difficult to constrain by observations, because it is an ill-posed problem with ambiguities concerning grain composition, lattice structure, size and shape distribution, and eventually dirty inclusions.

In this paper, we will argue for the formation of dirty dust grains in brown dwarf atmospheres from theoretical arguments. We consider the dust formation to take place in atmospheric upwinds powered by convective motions (see Helling 2003). The gas in these upwinds originates from the deep interior of the brown dwarf and is hence seed particle free – different from the condensation of water on aerosols in the Earth atmosphere. Therefore, the first process to occur in the dust formation circle must be the nucleation (seed particle formation) which requires much lower temperatures (higher supersaturation) as compared to the temperature where large solid particles are thermally stable. Once these seeds have formed, a large variety of condensible materials is already thermally stable, and different grain materials may grow on the surface on these seeds *simultaneously*. Thus, the formation of inhomogeneous dust particles with inclusions of different kinds of solid materials suggests itself.

Other theoretical works on dust formation in substellar atmospheres have not considered this basic problem. For example, dust formation is parameterised by a sedimentation efficiency $f_{\rm sed}$ in Ackerman & Marley (2001), by a critical temperature $T_{\rm cr}$ in Tsuji (2002), or by a maximum supersaturation ratio $S_{\rm max}$ in Cooper et al. (2003). The chemical homogeneity of the dust particles is always taken for granted, leading to well separated distributions of pure dust particles consisting of different materials, strictly following the dust stability sequence (see e.g. Lodders & Fegley 2005).

Based on such assumptions, static brown dwarf model atmospheres were developed which provided the first understanding of brown dwarf spectra (e.g. Allard et al. 2001; Tsuji 2002, and above cited works). Due to the parameterised treatment of dust formation, certain limiting cases needed to be considered, namely entirely dust enshrouded brown dwarfs (seemingly appropriate for spectral types ≈L2 . . . L4) and entirely dust

⋆ Appendices are only available in electronic form at http://www.edpsciences.org

cleared (settled) brown dwarf atmospheres (≈T1 . . . T9). The above mentioned parameterisation by Tsuji allows for first ideas to understand the L–T transition region (Tsuji 2005).

The present paper is the continuation of the work presented in Helling et al. (2001, 2004, Papers I and IV) and Woitke & Helling (2003, 2004, Papers II and III). Papers I and IV have investigated the key role of turbulence in the process of dust formation in substellar atmospheres on small spatial scales with a simple model for core-mantle grains. In Papers II and III, we have developed a large-scale quasi-static model for cloud layers in brown dwarf atmospheres including the evaporation and gravitational settling of size-dependent dust particles composed of one solid material. Helling et al. (2006) show a first study of the spectral appearance of such a chemically heterogeneous dust cloud layer.

In the present paper, we develop a kinetic description for the growth and evaporation of dirty dust particles (Sect. 2), which allows for a calculation of the time-dependent material composition of the dust grains and the consumption/enrichment of condensible elements in the gas phase. Section 3 describes an application of this theory to a small, actively condensing region in a brown dwarf atmosphere. In Sect. 4, we present our results and evaluate the influence of the sticking coefficient on our results. We discuss the need for seed particle formation and the possible consequences of dust formation for metallicity-determinations in Sect. 5, and draw our conclusive summary in Sect. 6.

2. Growth and evaporation of dirty grains

The dense, oxygen-rich gas of a substellar (e.g. brown dwarf) atmosphere consists of a variety of molecules (see Fig. 5) which can contribute simultaneously to the growth of different stable solid phases. We therefore expect the forming grains to consist of more than one solid material and to become patchy ("dirty"). If the surrounding temperature increases, for example because such a grain sinks downward in the atmosphere due to gravity, some of the solids start to become thermally unstable sooner than others, causing their evaporation.

Works in solid state physics show that the growth of one solid phase on another, already existing, alien solid surface results in aggregates of small islands (e.g. Chan et al. 2004). Chen et al. (2000) show, for instance, that copper islands form on TiO_2 surfaces, the size of which stays almost constant. The number of islands increases, if more copper settles on the surface. Furthermore, McCarty (2003) argues that solid islands shrink at a nearly constant rate during evaporation. Buyevich & Tre'yakov (1994) describe the formation of islands with a stochastic model showing that the supersaturation and the surface coverage by the new phase are functions of time.

In order to model the dust in brown dwarf atmospheres, we must describe both the growth and the evaporation processes quantitatively. The following assumptions are made (see Fig. 1):

Growth: the growth process proceeds via the following steps: 1) physisorption of impinging gaseous molecules on the total grain surface; 2) diffusive transport of these molecules via hopping to a solid island of suitable kind; and 3) surface chemical reaction and chemisorption at the surface of the island, i.e. creation of a new unit of that material and incorporation of this unit into the solid's crystal structure. We assume furthermore that the steps 2 and 3 proceed much faster than step 1, i.e. the growth rate of the solid islands is approximately given by the minimum of the physisorption rates of all required reactant molecules[1].

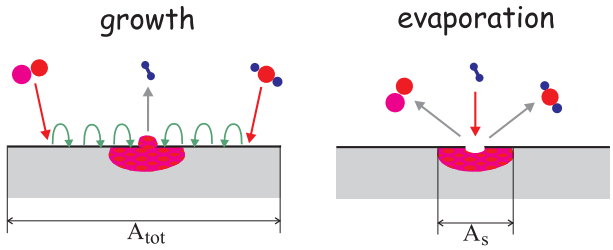

Fig. 1. Sketch of the surface chemical processes involved in the growth and evaporation of an island of solid material s at the surface of a dirty dust grain. The total surface area A_{tot} of the grain collects molecules which are then transported by hopping to meet on the island's surface area A_s, where the actual chemisorption process can take place.

Evaporation: we assume that the solid's evaporation process proceeds only from the surface of the islands of its own kind. These islands are assumed to be equally distributed on the surface as well as in the total volume of the grain, which will be denoted by "well-mixed" dust grains.

Experiments from solid state physics show that the heating of a compound of different solids first causes a inward/outward diffusion of the solid phases, i.e. a mixing of a possibly layered grain structure. Every evaporation process is initiated by such a diffusion since $E_{\rm diffus} < E_{\rm evap}$ (S. Schlemmer 2005, priv. com.). Therefore, whenever evaporation becomes important, the assumption of well-mixed grains seems justified.

In the following we will follow the basic idea of a dust moment method developed by Gail & Sedlmayr (1988)[2]. We express the evaporation rates of the different solid phases in a dirty grain by applying detailed balance considerations (Milne relations) to the growth rates with respect of a carefully defined reference state. We formulate the general problem in size space and define the dust moments in Sect. 2.1. The growth rates are quantified in Sect. 2.1.1 and the reference state is introduced in Sect. 2.1.2. Section 2.2 summarises the results for the modified growth velocity for dirty grains.

2.1. Master equation

We consider a size distribution of dirty dust grains denoted by $f(V)$ [cm^{-6}]. As argued in Dominik et al. (1993) it is favourable to work with the grain volume V instead of the grain radius or the monomer number as size coordinate in case of dirty grains. The master equation for the grains in size interval dV as affected by the various surface chemical reactions R, is given by

$$\frac{\partial}{\partial t}\Big(f(V)\,{\rm d}V\Big) + \nabla\Big(\boldsymbol{v}(V) f(V)\,{\rm d}V\Big) = \Big(R_\uparrow - R^\uparrow + R^\downarrow - R_\downarrow\Big)\,{\rm d}V, \quad (1)$$

where $\boldsymbol{v}(V)$ is the velocity of grains of size V. For simplicity, we will neglect drift velocities and identify $\boldsymbol{v}(V)$ with the hydrodynamic gas velocity $\boldsymbol{v}$ in this paper. How to include size-dependent particle drift is shown in Paper II. Multiplication of

[1] Hopping requires $E_{\rm therm} \lesssim E_{\rm physisorb}$, where $E_{\rm physisorb}$ is the binding energy of an alien ad-molecule on a solid surface. The efficiency of the hopping process depends hence on the temperature. If $E_{\rm therm}$ is too small, the arriving molecules can not move at the grains surface. If $E_{\rm therm}$ is too large, the just arrived molecule recoils from the surface (Gail & Sedlmayr 1984).

[2] Venables (1993) review such rate equation models discussing several experimental studies to show how these concepts can be applied.

Eq. (1) with $V^{j/3}$ ($j = 0, 1, 2, ...$) and integration over size results in

$$\frac{\partial}{\partial t}\Big(\rho\, L_j\Big) \;+\; \nabla\Big(\boldsymbol{v}\rho L_j\Big) = \int_{V_\ell}^{\infty}\Big(R_\uparrow - R^\uparrow + R^\downarrow - R_\downarrow\Big)V^{j/3}\,\mathrm{d}V, \tag{2}$$

where the dust moments $L_j(\boldsymbol{x}, t)[\mathrm{cm}^j/\mathrm{g}]$ are defined as

$$\rho L_j(\boldsymbol{x}, t) = \int_{V_\ell}^{\infty} f(V, \boldsymbol{x}, t)\, V^{j/3}\,\mathrm{d}V. \tag{3}$$

V_ℓ is the minimum volume of a large molecule ("cluster") to be counted as dust grain.

2.1.1. Growth rates

The Knudsen numbers are assumed to be appropriately large to consider a sub-sonic flow of freely impinging molecules to the grain surface (see Paper II for details). Furthermore, we will only consider type I surface reactions[3] in the main text of the paper. Type II and type III reactions are treated in detail in Appendix B. According to our assumptions outlined in Sect. 2, the growth (↑) and evaporation (↓) rates, which cause a (de-)population of the considered volume interval $[V, V + \Delta V]$ (see also Fig. 5 in Paper II), can be expressed by

$$R^\uparrow \mathrm{d}V \;=\; \sum_r f(V)\,\mathrm{d}V\, A_{\rm tot}(V)\, n_r v_r^{\rm rel}\alpha_r \tag{4}$$

$$R_\uparrow \mathrm{d}V \;=\; \sum_r f(V-\Delta V_r)\,\mathrm{d}V\, A_{\rm tot}(V-\Delta V_r)\, n_r v_r^{\rm rel}\alpha_r \tag{5}$$

$$R^\downarrow \mathrm{d}V \;=\; \sum_r f(V+\Delta V_r)\,\mathrm{d}V\, A_{\rm s}(V+\Delta V_r)\,\beta_r(V+\Delta V_r) \tag{6}$$

$$R_\downarrow \mathrm{d}V \;=\; \sum_r f(V)\,\mathrm{d}V\, A_{\rm s}(V)\,\beta_r(V). \tag{7}$$

$A_{\rm tot}(V)$ denotes the total surface area of the grain and $A_{\rm s}(V) = \sum_i A_{{\rm s}_i}$ the integrated surface area of all islands of solid s (i enumerates the islands of kind s). α_r is the sticking coefficient (ratio between physisorption rate and thermal collision rate) and β_r the evaporation rate coefficient of reaction r, respectively. n_r is the particle density of the key educt, which is the least abundant among the reactant molecules $k = 1 \ldots K$, and $v_r^{\rm rel}$ its thermal relative velocity. Strictly speaking, the key educt is identified by the minimum $\min\{n_k v_k^{\rm rel}\alpha_k/\nu_r^k\}$ among all educts of reaction r, where ν_r^k is the stoichiometric factor of educt k in reaction r. For further details, see Appendix B. Each reaction r leads to an increase (or decrease) of the dust grain volume by ΔV_r. Note that compared to Eqs. (59)–(62) in Paper II, we stay with the more general expressions of the surfaces area $A(V)$.

2.1.2. Reference state and Milne relation

In the following, we eliminate the evaporation rate coefficient β_r by a detailed balance consideration. In complete thermodynamic equilibrium, each process is exactly balanced by its reverse process. This reference state, which will be denoted by $^\circ$, is characterised by phase equilibrium with the considered solid ($S = 1$), which is in a pure state ($A_{\rm s} = A_{\rm tot}$) and has an infinite flat surface. Furthermore, thermal equilibrium between gas and solid ($T_{\rm g} = T_{\rm d}$), and chemical equilibrium in the gas phase ($n_r = n_r^{\rm CE}$) are valid. In this reference state, the growth and evaporation rates according Eqs. (4)–(7) are given by

$$\mathring{R}^\uparrow \mathrm{d}V \;=\; \sum_r \mathring{f}(V)\,\mathrm{d}V A_{\rm tot}(V)\,\mathring{n}_r \mathring{v}_r^{\rm rel}\,\mathring{\alpha}_r \tag{8}$$

$$\mathring{R}_\uparrow \mathrm{d}V \;=\; \sum_r \mathring{f}(V-\Delta V_r)\,\mathrm{d}V A_{\rm tot}(V-\Delta V_r)\,\mathring{n}_r \mathring{v}_r^{\rm rel}\,\mathring{\alpha}_r \tag{9}$$

$$\mathring{R}^\downarrow \mathrm{d}V \;=\; \sum_r \mathring{f}(V+\Delta V_r)\,\mathrm{d}V A_{\rm tot}(V+\Delta V_r)\mathring{\beta}_r(V+\Delta V_r) \tag{10}$$

$$\mathring{R}_\downarrow \mathrm{d}V \;=\; \sum_r \mathring{f}(V)\,\mathrm{d}V A_{\rm tot}(V)\mathring{\beta}_r(V). \tag{11}$$

First, we take advantage of the detailed balance $\mathring{R}_\uparrow = \mathring{R}_\downarrow$, which is valid even for each individual reaction r. Since the size distribution function of large clusters obeys in phase equilibrium $\mathring{f}(V - \Delta V_r) = \mathring{f}(V)$ (see Appendix A), we find

$$\mathring{\beta}_r(V) = \mathring{n}_r(T)\,\mathring{v}_r^{\rm rel}(T)\,\mathring{\alpha}_r\,\frac{A_{\rm tot}(V-\Delta V_r)}{A_{\rm tot}(V)}. \tag{12}$$

In an analogous way, $\mathring{R}^\uparrow = \mathring{R}^\downarrow$ leads to

$$\mathring{\beta}_r(V+\Delta V_r) = \mathring{n}_r(T)\,\mathring{v}_r^{\rm rel}(T)\,\mathring{\alpha}_r\,\frac{A_{\rm tot}(V)}{A_{\rm tot}(V+\Delta V_r)}. \tag{13}$$

Since rate coefficients (α, β) are universal material properties, which do not depend on the specific conditions in the local neighbourhood, we have found a general expression for the evaporation rate coefficient. Attention must be paid, however, to the temperature-dependence of β. Since we treat here the inverse of a monomer addition, the evaporation process is spontaneous, i.e. not triggered by a gas-grain collision (this is different for type II and type III surface reactions, see Patzer et al. 1998, and Appendix B). Hence, the evaporation process is completely controlled by the internal dust temperature and the proper Milne relation is $\beta(V) = \mathring{\beta}(V)|_{T=T_{\rm d}}$.

Inserting this Milne relation and the Eqs. (12) and (13) into Eqs. (4)–(7) leads to the following equations

$$R_\uparrow - R^\uparrow \;=\; \sum_r n_r v_r^{\rm rel}\alpha_r\Big(f(V-\Delta V_r)A_{\rm tot}(V-\Delta V_r) - f(V)A_{\rm tot}(V)\Big) \tag{14}$$

$$R^\downarrow - R_\downarrow \;=\; \sum_r \frac{\mathring{n}_r \mathring{v}_r^{\rm rel}\mathring{\alpha}_r}{b^{\rm s}_{\rm surf}}\Big(f(V+\Delta V_r)A_{\rm tot}(V) - f(V)A_{\rm tot}(V-\Delta V_r)\Big). \tag{15}$$

Using these intermediate results to evaluate the r.h.s. of Eq. (2) for sufficiently large ($V \geq V_\ell \gg \Delta V_r$) and spherical particles ($A_{\rm tot} = \sqrt[3]{36\pi}\,V^{2/3}$) yields with partial integration

$$\frac{\partial}{\partial t}\Big(\rho L_j\Big) + \nabla\Big(\boldsymbol{v}\rho L_j\Big) \;=\; \Big(V_\ell{}^{j/3} f(V_\ell) + \frac{\mathrm{j}}{3}\rho L_{j-1}\Big) \cdot \sqrt[3]{36\pi}\sum_r \Delta V_r\left(v_r n_r \alpha_r - \frac{\mathring{n}_r \mathring{v}_r^{\rm rel}\mathring{\alpha}_r}{b^{\rm s}_{\rm surf}}\right). \tag{16}$$

[3] For molecules M and grains S we define:
type I reaction: $M + S \leftrightarrows S'$
type II reaction: $M + S \leftrightarrows M' + S'$
type III reaction: $M_1 + M_2 + \ldots + M_j + S \leftrightarrows$
$(j > 1 \vee k > 1)$ $\leftrightarrows M_1' + M_2' + \ldots + M_k' + S'$.

Table 1. Chemical surface reactions r assumed to form one new unit of the solid material s in the grain mantel. The efficiency of the reaction is limited by the key species, which has the lowest abundance among the reactants. The notation ½ in the r.h.s. column means that only every second collision (and sticking) event initiates one reaction of kind r to form the dust species s (see $\nu_r^{\rm key}$ in Eqs. (24), (29)).

Index r	Solid s	Surface reaction	Key species (growth)
1	TiO_2[s]	$TiO_2 \longrightarrow TiO_2$[s]	TiO_2
2	rutile	$TiO + H_2O \longrightarrow TiO_2$[s] + H_2	TiO
3		$TiS + 2\,H_2O \longrightarrow TiO_2$[s] + $H_2S + H_2$	TiS
4	SiO_2[s]	$SiO_2 \longrightarrow SiO_2$[s]	SiO_2
5	silica	$SiO + H_2O \longrightarrow SiO_2$[s] + H_2	SiO
6		$SiS + 2\,H_2O \longrightarrow SiO_2$[s] + $H_2S + H_2$	SiS
7	Fe[s]	Fe $\longrightarrow$ Fe[s]	Fe
8	solid iron	$FeO + H_2 \longrightarrow$ Fe[s] + H_2O	FeO
9		$Fe(OH)_2 + H_2 \longrightarrow$ Fe[s] + $2\,H_2O$	$Fe(OH)_2$
10	Mg_2SiO_4[s]	$2\,Mg + SiO + 3\,H_2O \longrightarrow Mg_2SiO_4$[s] + $3\,H_2$	min{½Mg, SiO}
11	forsterite	$2\,Mg(OH)_2 + SiO \longrightarrow Mg_2SiO_4$[s] + $H_2O + H_2$	min{½$Mg(OH)_2$, SiO}
12		$2\,MgOH + SiO + H_2O \longrightarrow Mg_2SiO_4$[s] + $2\,H_2$	min{½MgOH, SiO}
13	Al_2O_3[s]	$2\,AlOH + H_2O \longrightarrow Al_2O_3$[s] + $2\,H_2$	½AlOH
14	corundum	$2\,AlH + 3\,H_2O \longrightarrow Al_2O_3$[s] + $4\,H_2$	½AlH
15		$Al_2O + 2\,H_2O \longrightarrow Al_2O_3$[s] + $2\,H_2$	Al_2O
16		$2\,AlS + 3\,H_2O \longrightarrow Al_2O_3$[s] + $2\,H_2S + H_2$	½AlS
17		$2\,AlO_2H \longrightarrow Al_2O_3$[s] + H_2O	½AlO_2H

The last factor in Eq. (16) can be expressed by means of the following identity

$$\frac{\mathring{n}_r \mathring{v}_r^{\rm rel} \mathring{\alpha}_r}{v_r n_r \alpha_r} = \frac{1}{S}\frac{1}{b_{{\rm chem},r}}\frac{1}{b_{{\rm therm},r}} \tag{17}$$

which is the ratio between the growth and the evaporation reaction rates of a pure solid. The supersaturation ratio S and the non-equilibrium b-factors are defined as

$$S = \frac{n_r^{\rm CE}(T_{\rm g}) k T_{\rm g}}{p_{\rm vap}^{\rm s}(T_{\rm d})} \quad \text{phase non-equil.} \tag{18}$$

$$b_{{\rm chem},r} = \frac{n_r}{n_r^{\rm CE}(T_{\rm g})} \quad \text{chemical non-equil.} \tag{19}$$

$$b_{{\rm therm},r} = \frac{\alpha_r}{\mathring{\alpha}_r}\sqrt{\frac{T_{\rm d}}{T_{\rm g}}} \quad \text{thermal non-equil.} \tag{20}$$

$$b_{\rm surf}^{\rm s} = \frac{A_{\rm tot}}{A_{\rm s}} \quad \text{surface area non-equil.} \tag{21}$$

Equations (18)–(21) express the effects of the different types of non-equilibria on the ratio between growth and evaporation rates. The explicit formulae for the supersaturation ratio S (see Appendix A) and the b-factors $b_{\rm therm}$ and $b_{\rm chem}$ are only valid for type I surface reactions.

For type II and type III reactions, the functional shape of the ratio between growth and evaporation rates (Eq. (17)) remains the same, but S must be replaced by a suitably defined reaction supersaturation ratio S_r and the explicit formulae for $b_{\rm therm}$ and $b_{\rm chem}$ are different (see Patzer et al. 1998 for type II reactions). The exact definition of S_r is given in Appendix B. In most cases, S_r is approximately given by a certain power of S, i.e. $S = S^{1/\nu_r^{\rm key}}$ (Eq. (B.8)). For the remainder of this paper, we will assume thermal and chemical equilibrium[4] and hence $b_{{\rm therm},r} = b_{{\rm chem},r} = 1$ for all surface reaction types.

[4] Due to the high densities in substellar atmospheres, deviations from thermal and chemical equilibrium are unlikely to occur, unless the atmosphere is illuminated from the outside. A fast collisional energy exchange between dust and gas is assured and hence $T_{\rm d} \approx T_{\rm g}$ (see Fig. 4 in Paper II).

2.2. The modified dust growth velocity

The remainder of the derivation of the dust moment equations is analog to Gail & Sedlmayr (1988). The result is

$$\frac{\partial}{\partial t}(\rho L_0) + \nabla(\boldsymbol{v}\rho L_0) = J(V_\ell) \tag{22}$$

$$\frac{\partial}{\partial t}(\rho L_j) + \nabla(\boldsymbol{v}\rho L_{\rm j}) = V_\ell{}^{j/3} J(V_\ell) + \frac{\rm j}{3}\chi^{\rm net}\rho L_{j-1}. \tag{23}$$

In case of net growth, $J(V_\ell) = f(V_\ell)\,\frac{{\rm d}V}{{\rm d}t}\big|_{V=V_\ell}$ can be identified with the stationary nucleation rate $J_\star$ (see Gail & Sedlmayr 1988, also Eq. (34)). Considering the special case of thermal and chemical equilibrium $b_{{\rm therm},r} = b_{{\rm chem},r} = 1$, the net growth velocity [cm/s] for dirty grains results to be

$$\chi^{\rm net} = \sqrt[3]{36\pi}\sum_s\sum_r \frac{\Delta V_r\, n_r v_r^{\rm rel}\alpha_r}{\nu_r^{\rm key}}\left(1 - \frac{1}{S_r}\frac{1}{b_{\rm surf}^{\rm s}}\right), \tag{24}$$

which takes into account the different surface areas responsible for growth and evaporation of all solid materials s incorporated into the dirty grains. $\nu_r^{\rm key}$ is the stoichiometric factor of the key reactant in reaction r (see Table 1).

According to our assumptions about the micro-physics of the growth and evaporation processes (see Sect. 2), the different solid islands can grow and evaporate simultaneously. Therefore, the net effect of single surface reactions (– growth or evaporation?) must be disentangled from the net effect for the entire dirty grain

	Reaction r	Entire grain
growth	$S_r b_{\rm surf}^{\rm s} > 1$	$\chi^{\rm net} > 0$
evaporation	$S_r b_{\rm surf}^{\rm s} < 1$	$\chi^{\rm net} < 0$

whereas in case of pure grains ($b_{\rm surf}^{\rm s} = 1$), the supersaturation ratio S alone determines the sign of *all* individual reactions (in thermal and chemical equilibrium), i.e. also the net effect for the growth or evaporation of dust grains.

2.3. Surface fractions and element conservation

For the following numerical simulations of the growth and evaporation of dirty grains we need to determine $b_{\rm surf}^{\rm s}$ for all

participating solid materials. As the most simple choice, we assume that all islands of all considered solid materials are well-mixed inside the dust grains

$$b^{\rm s}_{\rm surf} = \frac{A_{\rm tot}}{A_{\rm s}} = \lim_{a_1 \to a_2} \frac{V_{\rm tot}(a_2) - V_{\rm tot}(a_1)}{V_{\rm s}(a_2) - V_{\rm s}(a_1)} = \frac{V_{\rm tot}}{V_{\rm s}}, \quad (25)$$

i.e. we assume that $b^{\rm s}_{\rm surf}$ is independent of grain radius a and given by the volume fraction of material s.

Disregarding drift motions and diffusive mixing, the elemental composition of the dust component reflects the integral consumption of elements from the local gas $\Delta\epsilon_{\rm x}(t)$ since the onset of the dust formation process at $t = 0$. Assuming furthermore that there is a unique relation between the missing elements in the gas phase and the material composition of the grains we can write

$$V_{\rm tot} = \sum_{\rm s} V_{\rm s} \quad (26)$$

$$V_{\rm s} = V_{0,\rm s} \cdot \Delta\epsilon_{\rm x} \quad (27)$$

$$\Delta\epsilon_{\rm x}(t) = \epsilon_{\rm x,0} - \epsilon_{\rm x}(t), \quad (28)$$

where $\epsilon_{\rm x,0}$ is the initial abundance (here: solar) and $\epsilon_{\rm x}(t)$ the actual abundance of element x. $V_{0,\rm s}$ is the monomer volume of the solid s that forms from element x (see Appendix C).

The gas element conservation equations as affected by nucleation, growth and evaporation are given by

$$\frac{\partial}{\partial t}(n_{\langle \rm H\rangle}\epsilon_{\rm x}) + \nabla(\boldsymbol{v}\, n_{\langle \rm H\rangle}\epsilon_{\rm x}) = -\nu_{\rm x,0} N_l J(V_\ell) - \sqrt[3]{36\pi}\,\rho L_2 \sum_{r=1}^{R} \frac{\nu_{\rm x,s} n_r v_r^{\rm rel} \alpha_r}{\nu_r^{\rm key}} \left(1 - \frac{1}{S_r}\frac{1}{b^{\rm s}_{\rm surf}}\right) \quad (29)$$

with the total hydrogen nuclei density $n_{\langle \rm H\rangle}$ ($\rho = 1.424$ amu for solar abundances) and the stoichiometric coefficients $\nu_{\rm x,s}$ of element x in solid s. Consumption occurs due to nucleation (solid/liquid dust species $s = 0$) and due to net growth (reactions $r = 1 \ldots R$).

3. A demonstration for substellar atmospheres

Before we proceed to more complex applications of our theoretical approach in a forthcoming paper we will first discuss a simple as possible hydrodynamic set-up in order to illustrate the principle mechanisms and chemical feedbacks involved. We feel that this is necessary because of the complex interaction between chemical gas phase composition and dust formation process and their feedback on temperature and velocity field. For this purpose we also refrain from the complex turbulence model used in Paper IV but utilise the simple model of colliding expansion waves as used in Paper I. Our model represents an initially dust-free and hot ascending gas element in a brown dwarf atmosphere which is influenced by sound waves generated in the turbulent environment. At a first glance, this scenario seems very special. But in fact, astrophysical dust formation can be assumed to proceed always in a slowly cooling flow (e.g. Sedlmayr 1999), where turbulent variations will facilitate to overcome the nucleation barrier in most cases.

Section 3.1 summarises the complete set of model equations for a compressible, dust-forming gas. Section 3.2 describes the numerical features of the simulation code, initial and boundary conditions.

3.1. The model

Complex A: hydrodynamics. The hydrodynamical equations for an inviscid, compressible fluid with radiative cooling are

$$(\rho)_t + \nabla \cdot (\rho \boldsymbol{v}) = 0 \quad (30)$$

$$Sr\,(\rho \boldsymbol{v})_t + \nabla \cdot (\rho \boldsymbol{v} \circ \boldsymbol{v}) = -\frac{1}{\gamma M^2}\nabla P - \frac{1}{Fr^2}\rho \boldsymbol{g} \quad (31)$$

$$(\rho e)_t + \nabla \cdot (\boldsymbol{v}[\rho e + P]) = Rd_1\,\kappa(T^4_{\rm RE} - T^4), \quad (32)$$

with the caloric equation of state

$$\rho\, e = \gamma M^2 \left(\frac{\rho \boldsymbol{v}^2}{2} + \frac{1}{Fr^2}\rho g y\right) + \frac{P}{\gamma - 1} \quad (33)$$

with $\boldsymbol{g} = \{0, g, 0\}$. Radiative heating/cooling is treated by an relaxation ansatz with $T_{\rm RE}$ the radiative equilibrium temperature. The equations are written dimensionless by redefining each variable like $\zeta \rightarrow \zeta/\zeta_{\rm ref}$ with $\zeta \epsilon \{l, t, v, p, \rho, g, T, e\}$ being length, time, velocity, pressure, density, value of graviatational acceleration, temperature, and energy. The characteristic numbers build the respective reference values $M = v_{\rm ref}/c_{\rm s}$ ($c_{\rm s}$ – speed of sound), $Fr = v^2_{\rm ref}/(l_{\rm ref} g_{\rm ref})$, $Sr = l_{\rm ref}/(t_{\rm ref} v_{\rm ref})$, and $Rd_1 = 4\,\kappa_{\rm ref}\sigma T^4_{\rm ref} t_{\rm ref}/p_{\rm ref}$ (κ – total absorption coefficient). Latent heat release could be considered as an additional energy source for Eq. (32). According to the results of Woitke & Helling (2003) it can be neglected because it results in a maximum of $\Delta T = 1 \ldots 3.5$ K in the relevant grain size-density regim.

Complex B1: chemical equilibrium. In contrast to the hydrodynamic simulations presented in Papers I and IV, we calculate now the actual molecular abundances of our dust forming species in chemical equilibrium. We have implemented a chemical equilibrium routine involving 10 elements (H, C, N, O, S, Ti, Si, Mg, Fe, Al) which where chosen to cover the most important gas phase species for dust formation. We calculate the abundances of 36 molecules (H_2, N_2, NH_3, CH_4, HCN, CO, CO_2, H_2O, H_2S, SiS, SO, HS, SiO, SiH, SiH_4, SiO_2, SiN, SO_2, TiC, TiC_2, TiO, TiO_2, TiS, AlOH, AlO_2H, Al_2O, AlH, AlS, MgS, MgO, MgOH, MgH, $Mg(OH)_2$, FeO, FeS, $Fe(OH)_2$). We have checked that this reduced chemical equilibrium code yields approximately the same concentrations as the full chemical equilibrium code used in Paper II + III (14 elements and 155 molecules) with an error of less than about 10%. The molecular input data are the same and the element abundances applied are given in Appendix C.

Complex B2: dust formation. The dust formation including nucleation, growth and evaporation is modelled as described in Sect. 2. The system of equations is given in Sect. 2.2 and was solved in its dimensionless form.

We do only consider the formation of solid dust grains and our material quantities are not explicitely set to treat liquid phases.

The nucleation rate J_* is calculated for homogeneous $(TiO_2)_N$-clusters via

$$J_* = \frac{n_{\rm x}}{\tau} Z \exp\left[(N_* - 1)\ln S - \left(\frac{T_\Theta}{T}\right)\frac{(N_* - 1)}{(N_* - 1)^{1/3}}\right], \quad (34)$$

applying the modified classical nucleation theory of Gail et al. (1984). The seed growth time scale is $\tau^{-1} = n_{\rm x} v_{\rm rel,x} N_*^{2/3} A_0$ for a gaseous nucleation species x with a relative velocity $v_{\rm rel}$. $T_\Theta = 4\pi a_0^2 \sigma/k$ with a_0 being the hypothetical monomer radius

and with a value of the surface tension σ fitted to small cluster data based on quantum mechanical calculations of the cluster structures by (Jeong et al. 2000), see also Gail & Sedlmayr (1998) and Jeong et al. (2003)[5].

We consider the simultaneous growth of the solids TiO_2[s], SiO_2[s], Fe[s], Mg_2SiO_4[s] and Al_2O_3[s] onto the TiO_2 seed particles. The chemical surface reactions causing the growth and evaporation of these solids are listed in Table 1. We have selected these reactions to include all abundant reactants for a wide range of thermodynamic conditions (see Sect. 4.4.1). According to the number of solids formed, we have 5 blocks of chemical reactions. Many of the reactions involve also H_2O (as oxygen source) and H_2 (see Sect. 4.4).

It remains to specify the growth rate coefficients α, also called sticking coefficient. Andersen et al. (2003) have demonstrated the effect of this parameter on the mass loss efficiency of AGB stars. The mass loss rate increases with increasing sticking coefficient since dust forms faster. This conclusion is straightforward, it is not as straightforward to know the proper value for α for each of the chemical reactions r involved into the formation of the respective solid s (see Table 1). We follow the assumptions and citations in Paper I and use $\alpha_r = 1$ but discuss its implications in more detail in Sect. 4.6.

Complex B3: Element conservation. The element conservation is calculated according to Eq. (29) for the six affected elements O, Si, Mg, Fe, Al and Ti (+ sulphur S and hydrogen H) in their dimensionless form.

3.2. Numerics

Fully time-dependent solutions of the model equations have been obtained by applying a multi-dimensional hydro code (Smiljanovski et al. 1997) which has been extended in order to treat the complex of dust formation and element conservation (Helling et al. 2001). We solve 17 differential equation of which the energy equation, the dust moment equations, and the 8 element conservation equation (including S and H) can become very stiff due to the dust formation and its feedbacks.

Spatial dimension and grid resolution: for the purpose of this paper to demonstrate the temporal behaviour of an oxygen-rich gas forming dirty grains in a brown dwarf atmosphere, one-dimensional models are sufficient. The spatial resolution is 500 grid points and the size of the domain is $l_{\rm ref} = 10^5$ cm.

Model setup: the chosen parameters and initial conditions describe an initially hot and dust-free gas element in a slightly cooler, turbulent environment. The initial value for the gas temperature is chosen as $T_{\rm ref} = 1900$ K, which is above the temperature threshold for efficient nucleation of TiO_2 seeds. Two one-dimensional Gaussian-shaped isentropic pressure pulses with an arbitrarily chosen wavelength of $\lambda = 2.5$ m (simulating the turbulence) initiate temperature disturbances of order $\Delta T = -150$ K (see Figs. 2 and 4 in Paper I). The expansion waves temporarily induce a temperature drop below the temperature threshold for efficient nucleation. In contrast to Paper I, we chose the radiative background temperature $T_{\rm RE} = 0.9\,T_{\rm ref}$ to be above the nucleation threshold. Hence, efficient nucleation is only possible during the superposition phase of the expansion waves but thermal stability can be achieved also at later instants of time by radiative cooling.

[5] Note that e.g. Al_2O_3[s] can only be formed in the presence of a pre-existing surface, but is not considered as nucleation species due to the lack of a stable monomer Al_2O_3 in the gas phase (see Patzer 2004).

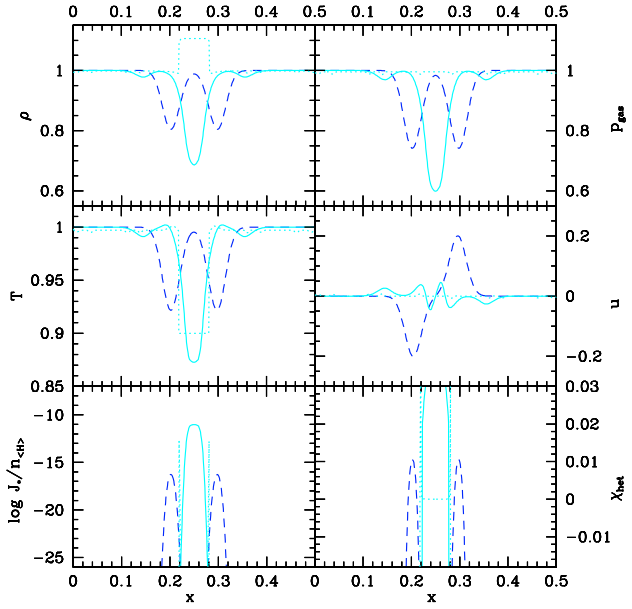

Fig. 2. Local hydro- and thermodynamical processes in a dust-forming gas as affected by expansion waves (dashed : 0.01 s, solid: 0.15 s, dotted: 5 s). *1st row*: l.h.s. density ρ, r.h.s. pressure p [dimensionless]. *2nd row*: l.h.s. temperature T, r.h.s. velocity u [dimensionless]. *3rd row*: l.h.s. nucleation rate $J_*/n_{\langle H\rangle}$ [1/s], r.h.s. net growth velocity $\chi^{\rm net}$ [cm/s]. *Parameter*: $T_{\rm ref} = 1900$ K, $T_{\rm RE} = 0.9 \times T_{\rm ref} = 1710$ K, $\rho_{\rm ref} = 10^{-3.5}$ g/cm^3 ($p_{\rm gas} = 2.15 \times 10^7$ dyn/cm^2, $n_{\langle H\rangle,\rm ref} = 1.35 \times 10^{20}$ cm^{-3}, M = 0.1 (Mach number), $t_{\rm ref} = 3.2365$ s, $l_{\rm ref} = 10^5$ cm).

Boundary conditions: the boundaries are transparanet and the same as in Paper I.

Initial conditions: the gas is assumed to contain initially neither seed nor dust particles $L_j(t = 0) = 0$. The element abundances are initially solar $\epsilon_{\rm x}(t = 0) = \epsilon_{\rm x,0}$. The gas temperature is initially homogeneous $T(t = 0) = T_{\rm ref}$, as are the pressure p and the mass density $\rho(t = 0) = \rho_{\rm ref}$. The velocity equals initially zero $u(t = 0) = 0$.

Material data: we use equilibrium constants fitted to the thermodynamical molecular data from the electronic version of the JANAF tables (Chase et al. 1985). The details on the material data for the dust complex are given in Appendix C. The gas and dust opacities are not treated in detail in this paper. We assume $\kappa_{\rm gas} = 10^{-3}$ cm^2/g and $\kappa_{\rm dust} = 1.17\pi\rho L_3\,T^{1.12}$ cm^2/g for astronomical silicates (Gail & Sedlmayr 1986) as in Paper I.

4. Numeric results

4.1. Hydrodynamics and dust formation

Figure 2 depicts the results for the simulation of an initially hot dust-hostile region of a substellar atmosphere (e.g. an ascending convective element) which is affected by expansion waves representing single turbulence events (eddies).

At the first depicted instant of time (dashed: 0.01 s, i.e. prior to the superposition of the two expansion waves) no or only very little nucleation takes place.

The second instant of time (solid: 0.15 s) shows the time of constructive superposition of the two expansion waves. The temperature falls below the nucleation threshold for TiO_2-seed formation, and the nucleation rate has a maximum. A considerable amount of small dust particles form ($n_{\rm d} \approx 10^7$ cm^{-3}) which enforce radiative cooling toward $T_{\rm RE}$ due to increased opacity.

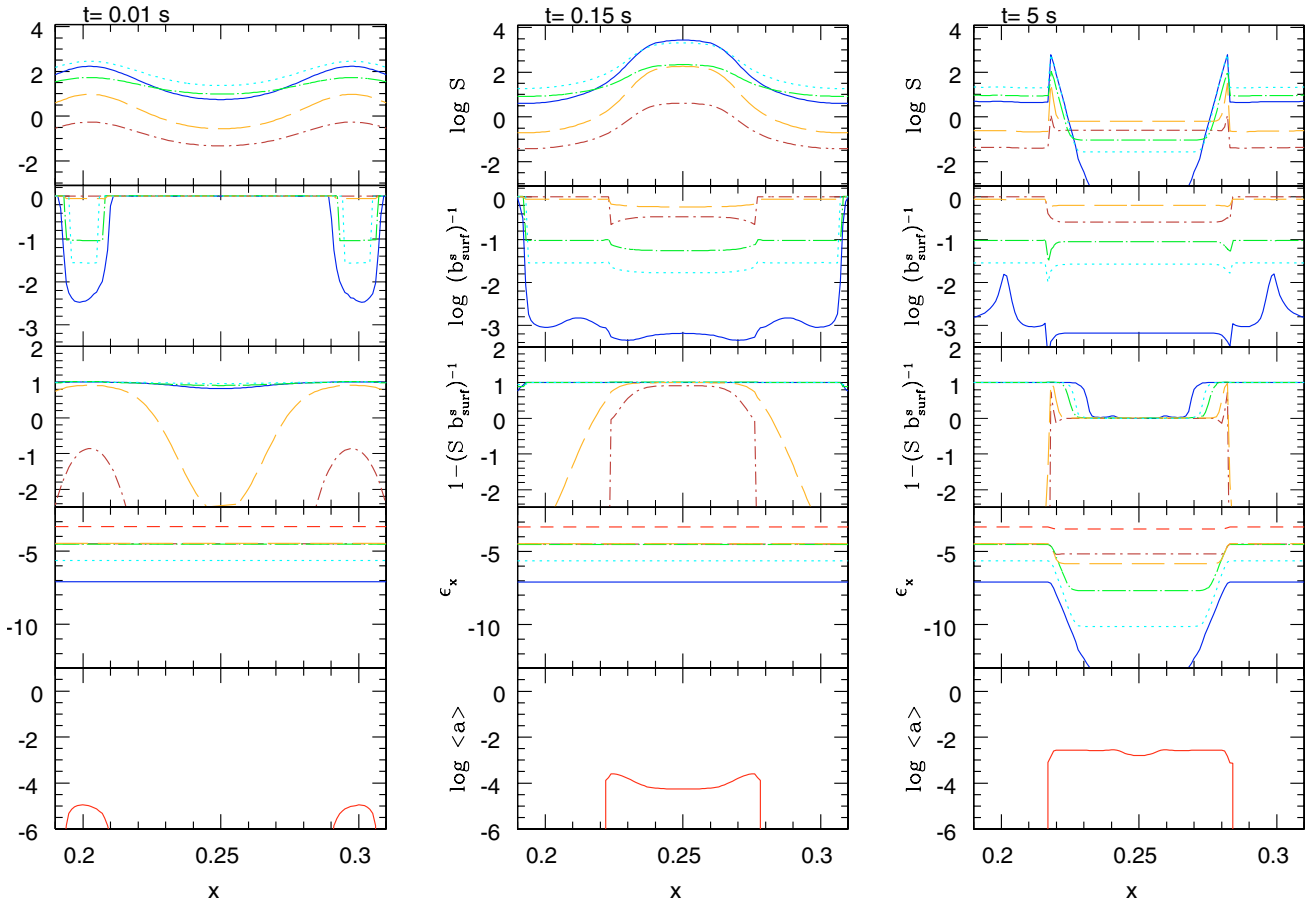

Fig. 3. Local details of the dust formation process and the evolution of the chemical abundances in the gas phase. The colours/line-styles indicate the dust species (and assigned elements) as follows. Dark blue/full: TiO_2[s] (Ti); brown/short dash-dot: SiO_2[s] (Si); green/long dash-dot: Fe[s] (Fe); orange/long dashed: Mg_2SiO_4[s] (Mg), light blue/dotted: Al_2O_3[s] (Al); red/dashed: [no assigned dust species] (O). *1st row*: supersaturation ratios S (*), *2nd row*: inverse surface area non-equilibrium factors $1/b^{\rm s}_{\rm surf}$, *3rd row*: factor determining growth or evaporation $1 - 1/(S\ b^{\rm s}_{\rm surf})$ (*), *4th row*: element abundances in the gas phase, *5th row*: mean dust particle size $\langle a \rangle$ [cm]. (*) Note, we plot $S^{1/2}$ for Al_2O_3[s] and Mg_2SiO_4[s] according to Appendix B.

Long after this superposition event (dotted: 5 s) the central dust formation site has reached a steady state characterised by pressure equilibrium, radiative equilibrium ($T \approx T_{\rm RE}$), and a phase equilibrium (see next paragraph).

4.2. Evolution of dirty grain formation

Figure 3 shows the results of the dust complex and the depletion of the gas phase for the same instants of time as depicted in Fig. 2, but only for the dust formation site, i.e. between $x = 0.2 \ldots 0.3$. Note that Fig. 3 dipicts S for all compounds but for Al_2O_2[s] and Mg_2SiO_4 $S^{1/\nu_{\rm r}^{\rm key}} = S^{1/2}$ ($\nu_{\rm r}^{\rm key} = 2$, see Table 1 and Appendix B) is plotted.

The first instant of time ($t = 0.01$ s, left column) shows the situation prior to the event of efficient nucleation. The most stable solid materials ($S \gg 1$ at $x = 0.25$) are Al_2O_3[s], Fe[s], and TiO_2[s] but the non-existence of seed particles hinders its condensation. The supersaturation of TiO_2[s] is not yet sufficiently high to initiate nucleation. Mg_2SiO_4[s] is thermally unstable ($S < 1$) in the region(s) not affected by the expansion waves. SiO_2[s] is everywhere thermally unstable. The gas abundances are throughout solar.

The second time step ($t = 0.15$ s, 2nd column) depicts the situation at the time of constructive superposition of the two expansion waves (compare caption Fig. 2). The corresponding temperature minimum results in a considerable increase of the supersaturation ratios, causing in this example the thermal stability of all considered solid materials. The reciprocal surface non-equilibrium factors $1/b^{\rm s}_{\rm surf} = V_{\rm s}/V_{\rm tot}$ indicate the volume fractions of the dirty grains. The growth rates of the different solid materials is mostly given by kinetic constraints (mainly the abundance of the key reactant). Mg_2SiO_4[s] growths the fastest followed by SiO_2[s], Fe[s], Al_2O_3[s] and TiO_2[s] is the slowest. The dust particles are still small ($\langle a \rangle \approx 1\,\mu$m) and the growth is not exhaustive yet. The gas abundances are still approximately solar.

The third time step ($t = 5$ s, right column) demonstrates the relaxation of the dust-forming system towards phase equilibrium. In the very centre of the superposition region, growth and evaporation already balance each other, hence $S\ b^{\rm s}_{\rm surf} \approx 1$ and $\chi^{\rm het} = 0$ for all reactions. Outside of the central region, further relaxation is still going on, where the growth of the solids becomes slower due to the decreasing abundances of the gaseous reactants via consumption. In the central region, the grains have reached their final size ($\langle a \rangle \approx 30\,\mu$m) with a material composition that is mainly given by element abundance constraints. Most of the dust volume is filled by Mg_2SiO_4[s], followed by SiO_2[s], Fe[s], Al_2O_3[s] and TiO_2[s]. The reduced element abundances reflect these amounts of condensates.

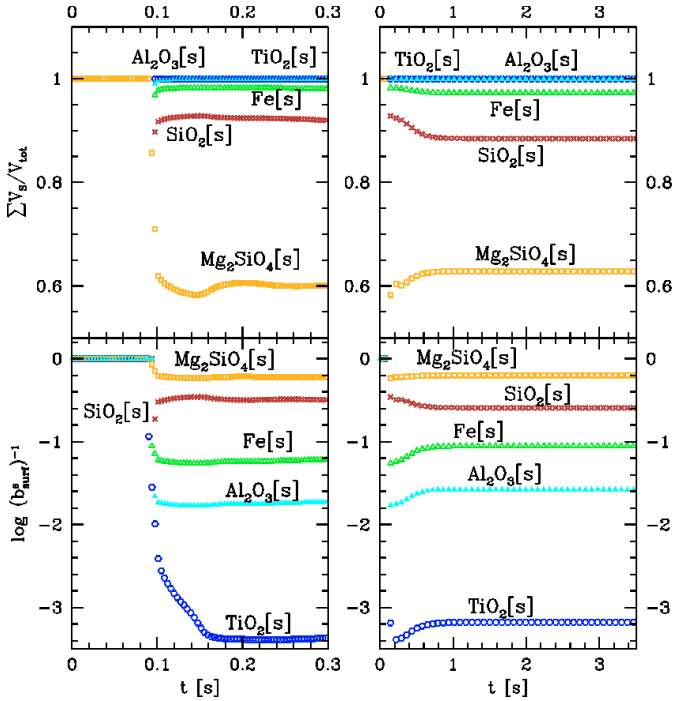

Fig. 4. Dust volume fractions, expressed by $1/b^{\rm s}_{\rm surf} = V_{\rm s}/V_{\rm tot}$, at the point of constructive wave interaction ($x = 0.25$) as function of time (*bottom panels*) and corresponding cumulative volumes $\sum V_{\rm s}/V_{\rm tot}$ (*top panels*). Orange/open squares: Mg_2SiO_4, brown/stars: $Mg_2SiO_4 + SiO_2$, green/open triangels: Mg_2SiO_4 + SiO_2 + Fe, light blue/filled triangles: $Mg_2SiO_4 + SiO_2 + Fe + Al_2O_3$, dark blue/open circles: $Mg_2SiO_4 + SiO_2 + Fe + Al_2O_3 + TiO_2$. *Left*: short-term behaviour, *right*: long-term behaviour. In the beginning, when dust is not yet present and $V_{\rm tot} = 0$, we put numerically $b^{\rm s}_{\rm surf} = 1$.

4.3. Dust material composition

Figure 4 depicts the dust volume fractions $1/b^{\rm s}_{\rm surf} = V_{\rm s}/V_{\rm tot}$ (Eq. (25)) as function of time for the five solid species taken into account Mg_2SiO_4[s], SiO_2[s], Fe[s], Al_2O_3[s], and TiO_2[s] (bottom panels). For a better overview, we also plot the cumulative volume fractions (upper panels).

Quickly after the onset of nucleation, the initial TiO_2 seed particles are covered by forsterite Mg_2SiO_4[s] (≈57%), silica SiO_2[s] (≈35%), with further inclusions of solid iron (≈5%) and corundum Al_2O_3[s] (≈2%). The rutile TiO_2[s] fraction is constantly decreasing with increasing grain size and finally negligible (<0.1%). Provided that the different solid materials are all sufficiently stable ($S \gg 1$), the rates of volume increase at early phases are *not* related to stability considerations. They are rather constrained by the following kinetic quantities: (i) the abundance of the key reactant for the growth reactions in the gas phase, (ii) its thermal velocity and (iii) the monomer volume of the respective solid.

The small wiggles in the SiO_2[s] and Mg_2SiO_4[s] volume fractions are related to the evolution of the temperature T (compare Fig. 6). The minimum temperature due to constructive superposition of expansion waves is achieved at $t \approx 0.15$ s. The radiative equilibrium temperatur is slightly higher and the forsterite Mg_2SiO_4[s] becomes temporarily thermally unstable and partly re-evaporate. The final composition in the relaxed phase equilibrium state ($S\, b^{\rm s}_{\rm surf} = 1$) favours Mg_2SiO_4[s] (≈64%) over SiO_2[s] (≈25%). The still relatively small contribution of solid iron (≈7%) is partly caused by its exceptionally small monomer volume (see Table B.1).

4.4. Evolution of gas phase composition

The composition of the gas phase is not only an important precondition for the process of dust formation, it is also a result of dust formation. Figure 6 shows the time evolution of the temperature, the chemical composition of the gas phase, and some dust quantities at the site of constructive wave superposition $x = 0.25$ (l.h.s.: short term – r.h.s.: long term).

In order to clarify the temperature dependence of the molecular concentrations, we have additionally plotted those concentrations as function of T in Fig. 5 for two sets of element abundances[6]. The l.h.s. of Fig. 5 shows the results for the initial (solar) element abundances, and the r.h.s. of Fig. 5 for those element abundances which are achieved at late stages in the dust formation model, when the dust-forming gas has reached phase equilibrium.

Consequently, not only supersaturation and surface coverage by the different solids are functions of time, as it was also shown by Buyevich & Tre'yakov (1994) who adopt a stochastic approach, also the remaining gas phase abundance vary with time.

4.4.1. Initial gas composition

The basis for the chemical composition of the gas phase is its element composition. Concerning the dust forming elements, oxygen (O) is initially most abundant, followed by iron (Fe), magnesium (Mg), silicon (Si), aluminum (Al), and titan (Ti). The carbon-to-oxygen ratio is C/O = 0.537 for the solar abundances given in Table C.1 according to Asplund et al. (2005). The resulting concentrations are shown on the l.h.s. of Fig. 5.

O complex: most of the oxygen is chemically bound into H_2O. The next most abundant oxygen carrier is CO down to about 1200 K (not depicted).

Fe complex: atomic iron is the most abundant iron species down to about 1150 K, where $Fe(OH)_2$ takes over. FeS, FeO and FeH (not depicted) are less important.

Mg complex: magnesium is most abundant in its atomic form down to about 1300 K, where MgOH and then $Mg(OH)_2$ become more abundant. MgH is also abundant at high temperatures. MgS, MgO and MgN are less important.

Si complex: SiO is clearly dominant, followed by SiS, down to about 800 K, where SiH_4 becomes the most abundant Si-species (not depicted). Silicon atoms and other silicon molecules (SiH, SiO_2, Si_2) are less important.

Al complex: the aluminium chemistry is complex. At higher temperatures, Al is mainly present in its atomic form, but already at about 2100 K, AlOH is more abundant than Al. Furthermore, AlO_2H and Al_2O are abundant molecules in the entire depicted T-interval. AlS and AlO are also abundant at high temperatures, and Al_2O_2 at very low temperatures. Other aluminum molecules like AlN and AlO_2 are less important.

Ti complex: at high temperatures, TiO is the most abundant Ti molecule, but already at 1600 K, TiO_2 becomes more abundant. Ti atoms and the TiS molecule are less important.

We conclude that in the temperature window 1800–1000 K, suitable for dust formation, atomic Fe (followed by $Fe(OH)_2$), atomic Mg (followed by $Mg(OH)_2$), SiO (followed by SiS), AlOH (followed by Al_2O) and TiO_2 (followed by TiO) can be

[6] Figure 5 has been calculated with the full chemical equilibrium code (14 elements and 155 molecules) which enables us to cross-check the reduced version of the chemical equilibrium code used during the hydrodynamic simulations.

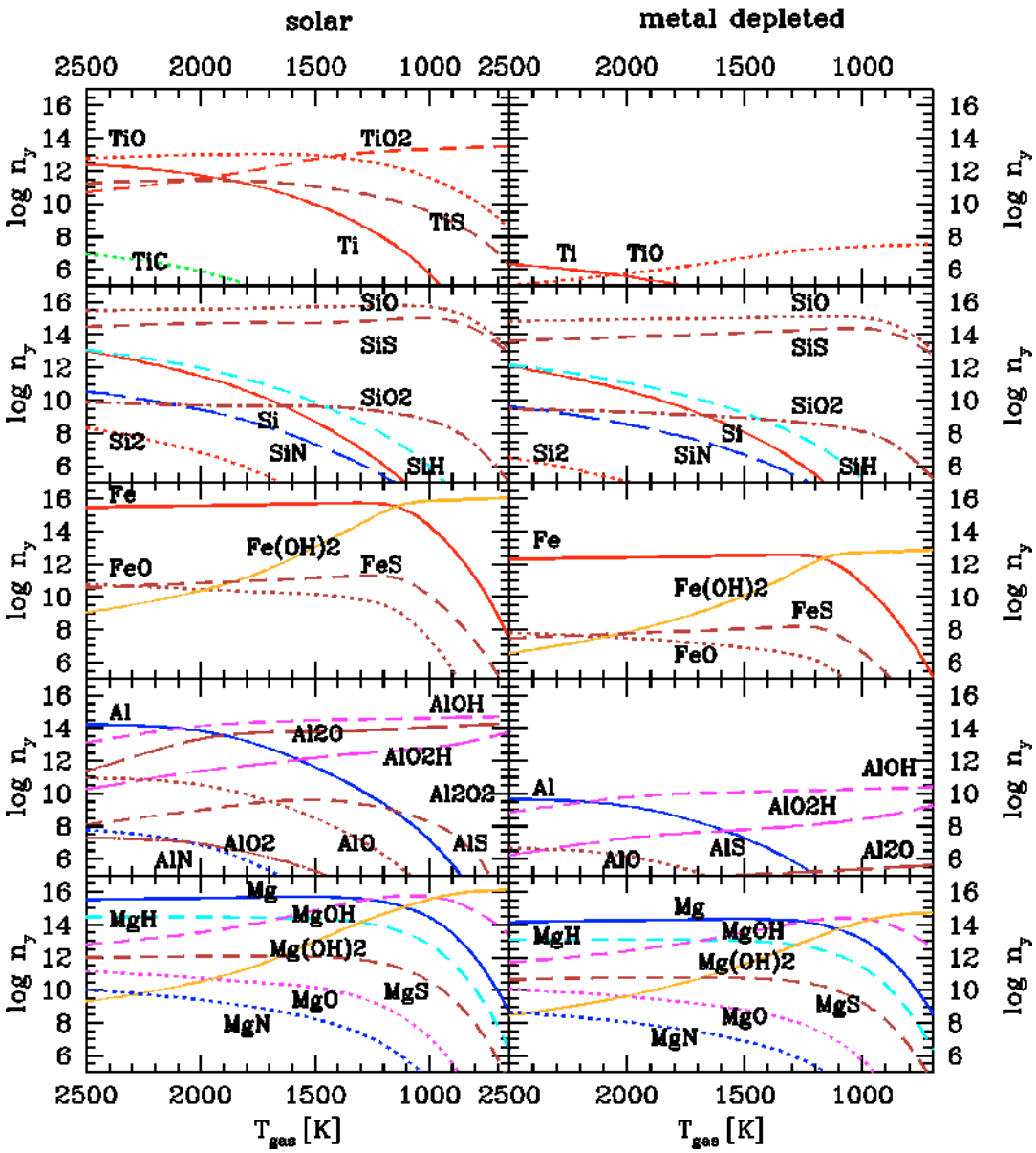

Fig. 5. Gas phase chemistry: particle densities n_y [cm^{-3}] as function of temperature T at $\rho = 10^{-3.5}$ g cm^{-3} ($p_{\rm gas} = 2.15 \times 10^7$ dyn/cm^2, $n_{\langle {\rm H} \rangle, {\rm ref}} = 1.35 \times 10^{20}$ cm^{-3}) for solar element abundances (l.h.s.) and for element abundances as present at late stages of the dust formation model (r.h.s.). These results are calculated with the complete chemical equilibrium code.

identified as the most important gaseous species for dust formation. The bulk solid phase is expected to form from these gaseous species.

These findings hold even for the metal-deficient case (r.h.s. of Fig. 5) where dust formation has reduced the metal abundances in the gas phase by many orders of magnitude. Polyatomic molecules with larger stoichiometric coefficients (e.g. Al_2O, TiO_2) are more affected by metal depletion. These conclusions have led us to the selection of the surface reactions listed in Table 1.

4.4.2. Early evolution of gas composition

During the early stages of dust formation (see l.h.s. of Fig. 6), the gas element abundances stay almost constant because the degrees of condensation $f_{\rm x}(t) = 1 - \epsilon_{\rm x}(t)/\epsilon_{\rm x,0}$ remain small. The evolution of the gas composition during these stages is mainly a consequence of the changing temperature, favouring more complex molecules as the temperature decreases. The growth time-scale of the different solid materials is rather similar.

4.4.3. Relaxation to phase equilibrium

After the formation of dust is completed (after about 0.5 s) the long-term behaviour of the element abundances and molecular concentrations are still affected by ongoing element depletion (r.h.s. of Fig. 6). An exponential decrease of the gas element abundances $\epsilon_{\rm x}(t)$ by about one (Si) to six (Ti) orders of magnitude is evident, until constant values are achieved at later stages. This behaviour results from a relaxation toward phase equilibrium characterised by $S\, b^{\rm s}_{\rm surf} = 1$, where the growth and evaporation reactions finally balance each other (see Sect. 2.1.2).

The time-scale for this relaxation can be derived from Eq. (29). Assuming that the growth process occurs at high supersaturation ratios ($S_r \gg 1$) and is dominated by a single growth reaction $\tilde{r}$ with a key reactant of maximum concentration

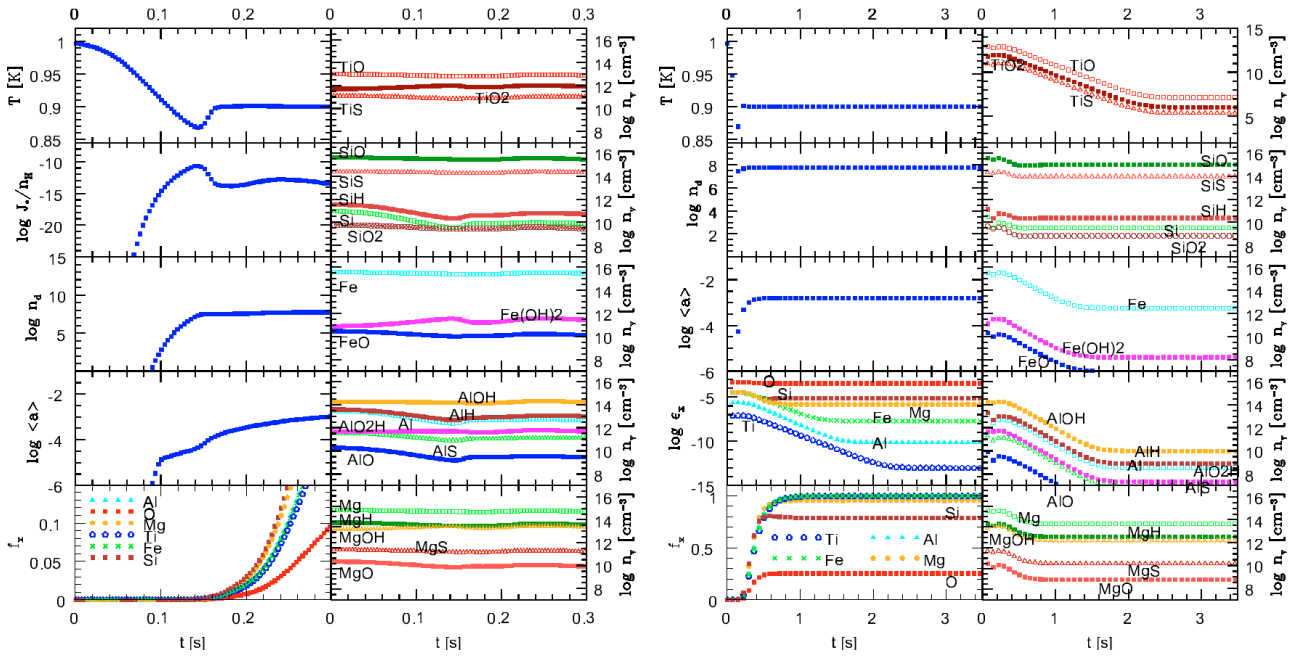

Fig. 6. Evolution of temperature, dust, and chemistry at the centre of wave interaction ($x = 0.25$, l.h.s.: short-term – r.h.s.: long-term). *Left panels on l.h.s.*: *1st row*: temperature T [1900 K], *2nd row*: nucleation rate per hydrogen nuclei $J_*/n_{\langle H\rangle}$ [1/s], *3rd row*: number of dust particles n_d [1/cm^3], *4th row*: mean grain radius $\langle a\rangle$ [cm], *5th row*: degree of condensation $f_x(t) = 1 - \epsilon_x(t)/\epsilon_{x,0}$ (red filled squares: O – orange filled hexagons: Mg – brown filled squares: Si – green crosses: Fe – cyan triangles: Al – dark blue open hexagons: Ti). *Left panels on r.h.s.*: *1st row*: temperature T [1900 K], *2nd row*: number of dust particles n_d [1/cm^3], *3rd row*: mean grain radius $\langle a\rangle$ [cm], *4th row*: element abundances ϵ_x *5th row*: degree of condensation $f_x(t)$ (same colour code). *Right panels*: number density of molecules n_y [cm^{-3}]. Note that the scaling on the l.h.s. and the r.h.s. is different.

$n_r = \epsilon_x n_{\langle H\rangle}$ (disregarding stoichiometry here), Eq. (29) can then be written as

$$\frac{d\epsilon_x}{dt} = -\sqrt[3]{36\pi}\,\rho L_2\,\epsilon_x v_{\tilde{r}}^{\rm rel}\alpha_{\tilde{r}}. \qquad (35)$$

The depletion time-scale towards phase equilibrium is hence

$$\frac{1}{\tau_{\epsilon_x}^{\rm depl}} = \sqrt[3]{36\pi}\,\rho L_2\, v_{\tilde{r}}^{\rm rel}\alpha_{\tilde{r}}. \qquad (36)$$

Since the total surface area of the dust component $\sqrt[3]{36\pi}\rho L_2$ is unique for all elements (according to our assumptions about the growth of dirty grains), the difference between the depletion time-scale of different elements is either a consequence of different thermal relative velocities $v_{\tilde{r}}^{\rm rel}$ or different sticking coefficient $\alpha_{\tilde{r}}$.

The final values for the degrees of condensation depend strongly on the final temperature in the medium (the final atmospheric height of the ascending convective element) as known from phase equilibrium calculations (see e.g. Sharp & Hübner 1990). For the chosen value for $T_{\rm RE} = 0.9 \times 1900\,{\rm K} = 1710\,{\rm K}$, SiO_2[s] is not very stable, resulting in final degrees of condensation of only about 80% for Si, and Mg reaches only 95%. In contrast, Al_2O_3[s], Fe[s] and TiO_2[s] are more stable, resulting in almost 100% condensation of Al, Fe and Ti. The degree of condensation of oxygen remains small (about 20%), however increasing the C/O ratio from initially 0.537 to finally 0.719.

It is noteworthy that although the dust formation process is quickly completed (n_d = const. after 0.14 s, $\langle a\rangle$ = const. after 0.4 s, f_x = const. after 1 s) the depletion of the element abundances takes more time (up to 2.2 s for Ti), if the initial and final values for the respective gas element abundance differ by many orders of magnitude, which takes many $\tau_{\epsilon_x}^{\rm depl}$.

4.5. Moving upward toward lower temperatures

An ascending convective gas element in a brown dwarf atmosphere always moves along the direction of decreasing temperature, until it cools and dissolves in the surrounding gas, finally achieving the thermodynamical conditions of the ambient gas. Estimates for typical convective turn-over time-scales result in $\tau_{\rm conv} = H_p/v_{\rm conv} \approx 20\,{\rm min}$ ($H_p = 10^6$ cm, $v_{\rm conv} = 10^3$ cm/s).

In the course of the dust formation process in such a plum or bubble, radiative cooling occurs with increasing efficiency as the amount of dust increases. For the situation considered (caption Fig. 2) the radiative cooling time-scale ranges from $\tau_{\rm rad} = 2\,{\rm s}$ without dust formation and $\tau_{\rm rad} = 0.06\,{\rm s}$ with dust formation, if the plum is considered to radiate like a black body (Eq. (25) in Paper I and $\kappa_{\rm gas} = 10^{-3}$ cm^{-1}, $\kappa_{\rm dust} = 10^{-1.5}$ cm^{-1})[7,8]. Hence, the gas / dust mixture will reach fast the radiative equilibrium temperature $T_{\rm RE}$ also if it is considerably smaller than the temperature from which such a convective element originates, i.e. in our case $T_{\rm ref}$.

So far we have studied the results for convective plums or bubbles that do not ascend very high in the atmosphere ($T_{\rm RE} = 0.9 \times T_{\rm ref} = 1710\,{\rm K}$). Now we demonstrate the results for $T_{\rm RE} = 0.5 \times T_{\rm ref} = 950\,{\rm K}$, simulating dust-forming bubbles that reach much higher layers (Fig. 7).

The principle evolution of dust and gas is similar compared to the previous case. However, the nucleation rate reaches higher values, which causes the creation of about 10^3 times more dust particles in comparison to the previous case, which therefore remain much smaller $\langle a\rangle \lesssim 1\,\mu$m. The intermediate minimum of

[7] Note the error in the $\tau_{\rm rad}$ estimation in Eq. (25) in Paper I.

[8] The exact value depends on the definition of the cooling time-scale considered. If $\tau_{\rm cool} = \|e_{\rm th}/Q_{\rm rad}\| = p/((\gamma-1)\cdot\rho 4\sigma\cdot\cdot(\kappa/\rho)\cdot(T_{\rm RE}^4 - T^4))$, it follows $\tau_{\rm cool} = 16\,{\rm s}$ and $0.53\,{\rm s}$ without and with dust, respectively.

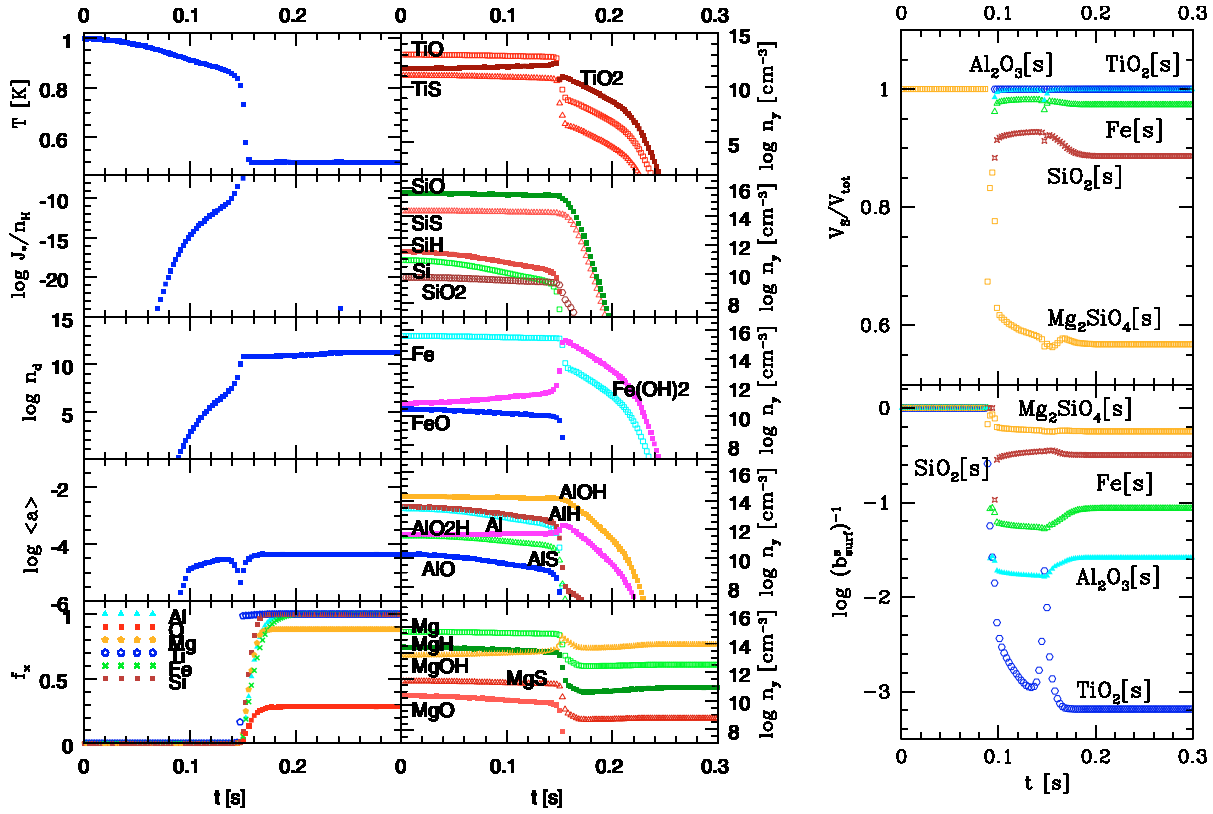

Fig. 7. Same as l.h.s of Figs. 6 and 4, but for $T_{\rm RE} = 0.5 \times T_{\rm ref} = 950$ K, simulating an convective element that ascends to a higher atmospheric latitude. *Left*: time evolution of temperature, dust, and chemistry. *Right*: time evolution of the cumulative volumes $\sum V_{\rm s}/V_{\rm tot}$ (*top*) and the solid volume fractions $1/b^{\rm s}_{\rm surf} = V_{\rm s}/V_{\rm tot}$ (*bottom*).

$\langle a \rangle$ at $t \approx 0.15$ s is a consequence of this fast production of seed particles. Such a distribution of small grains results in a much larger total surface area of the dust component $\sqrt[3]{36\pi\rho L_2}$ which eventually accelerates all growth and evaporation processes.

Consequently, the dust formation is completed very rapidly ($\Delta t \approx 0.05$ s) after the maximum of nucleation has occurred at $t \approx 0.15$ s. Also the subsequent depletion of the gas phase proceeds faster. The gas phase is virtually free of Si, Al, Fe, and Ti after about 0.18 s. Now, Mg_2SiO_3[s] is the last stable which result in a final degree of condensation of only ≈90% for Mg. The rapid temperature drop to $T_{\rm RE} = 950$ K causes also a considerable change of the chemical composition of the gas phase. Complex molecules like $Fe(OH)_2$ and AlO_2H become very abundant. This temperature effect is partly masked by the influence of the decreasing gas phase element abundances.

The r.h.s. of Fig. 7 shows the resulting material composition of the dust particles, close to phase equilibrium. The majority of Si disappears in Mg_2SiO_4[s] which is in competition with the SiO_2[s] formation. The consequence is the incomplete condensation of Mg. The final dust volume composition according to the present model is about 56% Mg_2SiO_4[s], ≈32% SiO_2[s], 8% Fe[s], 1% Al_2O_3[s] and <0.1% TiO_2[s]. The fraction of Mg_2SiO_4[s] did decrease somewhat in favour of SiO_2[s] compared to the hotter case in Sect. 4.3. This is a tendency relevant for the spectral appearance of dust cloud layers where the uppermost, cool layers will mostly influence the IR spectrum.

4.6. Influence of material quantities: the sticking coefficient

We have presented results from our theoretical model of oxygen-rich heterogeneous dust formation. Major input properties for every model are material quantities. The sticking coefficient α_r is such an input value to our dust formation model and it describes the efficiency of a chemical surface reactions r to contribute to the growth of the grain mantle (Sect. 2.1.1). One source to obtain these values are experiments and only a few seem to exist for non-icy particles. Hashimoto (1990) considers the destruction of Mg_2SiO_4[s] and summarized $\alpha^{\rm SiO_2} \approx 0.01$ for SiO_2[s] ⟶ SiO + O, $\alpha^{\rm SiO_2} \approx 1$ for SiO_2[s] ⟶ SiO_2 ($r = 4, 5$ in Table 1), $\alpha^{\rm Mg_2SiO_4} \approx 0.04$, and $\alpha^{\rm metall} \approx 1$. Hence, the formation of Mg_2SiO_4[s] and SiO_2[s] has to overcome a reaction barrier while metals do not. The experiments by Nagahara & Ozawa (1996) suggest $\alpha^{\rm Mg_2SiO_4} \approx 0.1$. Obeying the facts that experimental data differ and that the sticking process would also depend on details like the structure of the already existing surface and its temperature, we performed test calculation to illustrate the principle influence of the sticking coefficients on the results presented in Sect. 4. Case #0 is the standard setting of this paper, case #1 considers SiO_2[s] and Mg_2SiO_4[s] with similar $\alpha < 1$, case #2 has a decreased α for one of the SiO_2[s] reactions, and case #4 resembles the most extreme values given in Hashimito (1990).

In principle, a decreasing sticking coefficient causes a decreasing growth speed. We demonstrate this for the cumulative volume fraction $\sum V_{\rm s}/V_{\rm tot}$ and the degree of condensation $f_{\rm x}$ in Fig. 8, because $V_{\rm s}/V_{\rm tot}$ is linked to the spectral appearance of a dust cloud layer, $f_{\rm x}$ demonstrates the influence on the gas phase chemistry.

We observe a difference in the short-term (l.h.s.) and in the long-term (r.h.s.) behavior of our dust forming system. The short-term behavior is influenced by the dust kinetics, therefore large differences occur between the case #0 ($\alpha = 1$) and the other

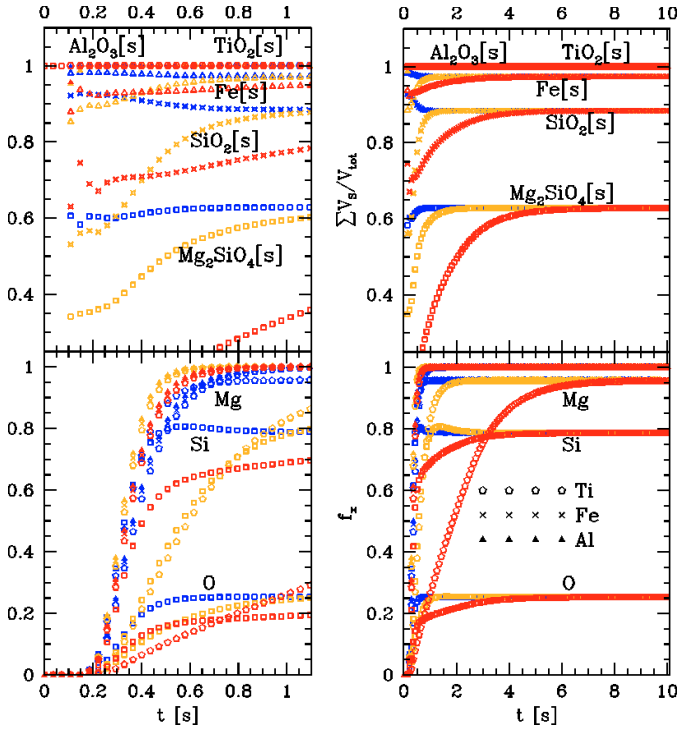

Fig. 8. Influence of reaction kinetics on the cumulative volume fraction $\sum V_s/V_{tot}$ (*top*: open squares: Mg_2SiO_4, Stars: Mg_2SiO_4 + SiO_2, Open triangles: $Mg_2SiO_4 + SiO_2 + Fe$, Filled triangles: $Mg_2SiO_4 + SiO_2 + Fe + Al_2O_3$, Open circles: Mg_2SiO_4 + SiO_2 + Fe + Al_2O_3 + TiO_2.) and the degree of condensation f_x (*bottom*). Different cases are colour coded: case #0 – dark blue, case #1 – light blue (just below orange), case #2 – orange, case #3 – red (Table 2).

Table 2. Influence of the sticking coefficients. For reaction index r see Table 1.

Index r		#0[1]	#1	#2	#3[2]
1, 2, 3[3]	$\alpha^{TiO_2}_{1,2,3}$	1	1	1	1
4	$\alpha^{SiO_2}_{4}$	1	0.1	0.1	1
5	$\alpha^{SiO_2}_{5}$	1	0.1	0.01	0.01
6 [3]	$\alpha^{SiO_2}_{6}$	1	0.1	0.1	1
7, 8, 9	$\alpha^{Fe}_{7,8,9}$	1	1	1	1
10, 11, 12	$\alpha^{Mg_2SiO_4}_{10...12}$	1	0.1	0.1	0.04
13 ... 17 [3]	$\alpha^{Al_2O_3}_{13...17}$	1 [dark blue]	1 [light blue]	1 [orange]	1 [red]

[1] Resembles Sect. 4. [2] The most extreme values given in Hashimoto (1990). [3] No measurements in the literature. We assume $\alpha = 1$ for TiO_2[s], Al_2O_3[s] and $\alpha^{SiO_2}_4 = \alpha^{SiO_2}_6$.

cases where $\alpha < 1$. The results for case #1 and case #2 are very similar because α differs for only one reaction ($r = 5$). The relaxation towards phase equilibrium takes longer the smaller the sticking coefficients are (case #0 → case #1 and #2 → case #3). Case #3 considers the smallest α for the two major dust compounds SiO_2[s] and Mg_2SiO_4[s], and hence, has the longest relaxation time. The slowest relaxation occurs for the Mg-complex in case #3 because all Mg_2SiO_4-reactions proceed with the same, low α, in contrast to SiO_2[s] where only one reaction has a comparably small α. It becomes, however, clear that one slow compound influences the relaxation towards phase equilibrium of the whole dust chemistry. Figure 8 illustrates that the actual relaxation time depends very much on the values of the sticking coefficient which is not known for part of the reactions, or which has large uncertainties as stated by Hashimoto (1990) for $\alpha^{SiO_2}_5$, or for which different experiments result in different values ($\alpha^{Mg_2SiO_4}$: Hashimoto 1990; Nagahara & Ozawa 1996).

Eventually the system reaches phase equilibrium and the results are the same in all four cases (r.h.s. Fig. 8) including gas phase depletion.

5. Discussion

5.1. The need for seed particle formation in brown dwarfs and giant gas planets

The thermo- and hydrodynamic conditions in brown dwarf atmospheres may at first appear similar to the Earth's atmosphere, which raises an important and repeatedly asked question. Namely, if seed formation is really an important issue for the formation of dust in brown dwarfs and gas giant planets.

The formation of water droplets in the Earth atmosphere is triggered by the presence of so-called aerosols. Aerosols are very small liquid or solid particles, which remain suspended over a long period of time since they are thermally stable and their drift velocities are very small. Aerosols are for instance volcanic dust particles injected into the atmosphere by the most violent eruptions (e.g. El Chichon, Mexico 1982, temporal albedo increase of 10%). Another way of aerosol production is fire in the tropics, smoke-tracks, and tire particles. The main Earth aerosols, however, are H_2SO_4-water droplets (0.001 ... 1 μm) from sulphur release by volcanoes, coal burning, and decomposition of organic matter (Traub 2005, priv. com.). All these aerosols serve as seed particles – maybe coated with patches of sulfur (Korhonen et al. 2003) – for formation of water droplets and can be washed out from the terrestrial atmosphere by rain. If there are many of such seeding aerosols, the number of liquid droplets increases, and the size of the rain droplets decreases (compare J_*, n_d, $\langle a \rangle$ between Figs. 6 and 7), which enables these particles to sustain longer in the atmosphere since their gravitational drift velocities are smaller.

Brown dwarfs and giant gas planets do not provide any of the aforementioned mechanisms for seed particle formation. Instead, both constantly mix up hot gas from the deep interior, where the thermal stability of solids and liquids is not provided, into the atmosphere. This changes the picture of rain formation known from the Earth atmosphere considerably. In brown dwarf atmosphere, the dust formation happens in upwinds just at those temperatures where the very first seed particles can be formed, making the nucleation and the influence of turbulence on the nucleation to key issues for the discussion of dust formation in brown dwarf atmospheres.

The situation in giant gas planets, which can be much cooler, will be again different. Here, the same dust formation processes may occur in very deep layers, but the observable surface layers are so cool that the formation of more volatile species like ice particles becomes important. The formation of such secondary particles must be discussed on top of the refractory grain formation in deeper layers. The refractory dust particles, as considered in this paper, will probably serve as seeds for the more volatile species in the upper atmosphere.

5.2. Primordial versus processed metallicity

Burgasser (2004) and Burgasser et al. (2004) have presented evidence (i.e. high proper motions) for the discovery of halo brown dwarfs. Halo brown dwarfs are old objects, which suggests that they are primordially metal poor and that they have probably all cooled into the T dwarf regime, as for example the 2MASS brown dwarf 0034+0523 (Burgasser et al. 2004). Hence, they should exhibit an even stronger metal deficiency than other halo stars or stars in the galactic plane of similar age because of the additional metal depletion by dust formation and settling in brown dwarfs.

According to the results of this paper, this additional metal depletion by dust formation, which could mimic primordial metal abundances, is very difficult to determine by models. The depletion time-scale is the longest among all chemical and dust formation time-scales, which suggests that *phase equilibrium is not valid in the outer layers* (see Helling et al. 2005; and conclusions of Paper III). Due to the ongoing mixing, the depletion is expected to be incomplete which means that a lot more metal carrying molecules like FeH, CaH and TiO can be present in comparison to phase equilibrium.

Dust formation will proceed via every available chemical channel and therefore influence the element abundance of almost every species. Exceptions being the noble gases, hydrogen and maybe some peculiar elements which do not possess a stable solid phase. A possible way out of this masking effect might be that in case of primordial stars, all metal abundances should be approximately reduced by some constant factor. Dust formation, in contrast, discriminates strongly between different metals. The results of this paper, for example, suggests that Al and Fe should be much more depleted than Si and Mg. Lodders & Fegley (2005) have suggested that if GeH_4 can be detected instead of SiH_4, and H_2S can be detected instead of Fe binding molecules, the metal deficiency in very cool objects should be caused by dust consumption.

Cowan et al. (2005) suggested a metal abundance of $-3.1 \lesssim$ [Fe/H] $\lesssim -1.6$ for galactic halo giant stars, and [Fe/H] > -1 for galactic disk stars (Cowan et al. 2002). Extreme sub-dwarfs are known to have [Fe/H] $\sim -2.0 \pm 0.5$ (Gizis et al. 1997). For comparison, the differences of metal element abundances $\Delta\epsilon_x$ due to our dust formation model (see Fig. 6) are [Ti/H] $= -6$, [Fe/H] $= -3$, [Al/H] $= -4$, [Mg/H] $= -1$, [Si/H] $= -0.5$ in the final state, which is per definition the logarithmic difference to the solar, i.e. our initial, values. Obviously, these deficiencies are not of similar orders of magnitude and not correlated with iron. It follows that a brown dwarf atmosphere with a chemical composition as calculated from our model could in fact mimic primordial low metal abundances.

6. Conclusive summary

We have proposed a model for the formation of dirty dust particles in brown dwarf atmospheres, which consist of numerous small islands of different solid materials like Mg_2SiO_4[s], SiO_2[s], Al_2O_3[s], Fe[s] and TiO_2[s]. This idea is supported by experimental findings (Sect. 2) and observations of coated terrestrial dust particles (see Korhonen et al. 2003). Assuming that the impinging molecules are rapidly transported by hopping on the surface to the respective solid islands, we have derived a general moment method for the treatment of nucleation, growth and evaporation for such dirty grains with an oxygen-rich element composition. Our approach allows to determine the time-dependent size distribution and solid material composition of the dirty grains, and the time-dependent chemical composition of the gas phase.

Our model is motivated by laboratory results and by the necessity of the key process of nucleation (seed particle formation) to occur first. In order to stabilise small clusters in the gas phase and so to initiate the nucleation process, low temperatures must be achieved (causing the required supersaturation). At such temperatures, a variety of solid materials is already thermally stable which suggests that if seed particles are once formed, they will be immediately covered by different solid materials in a simultaneous way, which results in dirty grains.

In order to overcome this nucleation barrier, turbulence is an important issue which may temporarily provide the required low temperatures, e.g. by the superposition of expansion waves. Locally higher nucleation rates result in smaller grains which sustain longer in the atmosphere since their gravitational drift velocities (gravitational settling) are smaller. Thus, the proposed turbulent scenario for dust formation leads to a patchy, non-uniform distribution of dust with e.g. a spatially varying size and material distribution.

In application to convective gas elements that ascend in the brown dwarf atmosphere, radiative cooling is also important for the dust formation. Such ascending bubbles are hotter than in radiative equilibrium. Consequently, if once dust forms and the opacity of the gas/dust mixture increases, radiative cooling causes a rapid decrease of the temperature which influences the resulting dust quantities.

Considering typical densities of $10^{-3.5}$ g cm^{-3} in brown dwarf atmospheres, the dust formation process results to be fast (between 0.1 s and 0.5 s), but the consumption of metal atoms from the gas phase takes longer, which suggests that the gas phase depletion by dust formation can be incomplete, i.e. less than predicted by phase equilibrium models. Together with the patchy, non-uniform appearance of the dust due to turbulence, the incomplete depletion makes metallicity measurements highly uncertain.

The initial dust growth phase after nucleation onset proceeds far away from phase equilibrium and the resulting solid material composition of the dirty dust particles are at first given by kinetic constraints. However, at later stages, when the gas phase is strongly depleted, the material composition of the grains is actually *not* frozen in, but less stable materials like SiO_2[s] and Mg_2SiO_4[s] slowly evaporate and the newly liberated metals can form other, more stable condensates at low temperatures at radiative equilibrium level. In this way, the material composition of the dust particles approaches final values as known from phase equilibrium considerations.

The final solid material composition of the dirty dust grains depends hence strongly on the temperature in the respective atmospheric layer. Considering a temperature interval from $T_{\rm RE} = 1710\,{\rm K} \rightarrow 950\,{\rm K}$, we find changing volume fractions of the considered solid materials. The fractions of silica SiO_2[s] and solid iron Fe[s] increased on the cost of Mg_2SiO_4[s].

The dust formation leads to different degrees of gas phase depletion for different elements. This selective nature of the dust formation may help to disentangle primordial from dust-affected metallicities.

Acknowledgements. We thank the referees, Dr. Joseph Nuth III and Dr. Erwin Sedlmayr for interesting suggestions to the manuscript. We thank Stephan Schlemmer and Wing-Fai Thi for enlightning discussion on the mansucrip's subject. W. A. Taub is thanked for sharing his knowledge on aerosols with us. Ch.H. acknowledges the *Berliner Programm zur Förderung der Chancengleichheit von Frauen in Wissenschaft und Lehre* and the ESA Research Fellowship program at ESTEC in Noordwijk. P.W. has been supported in the frame of the

AstroHydro3D initiative by the NWO Computational Physics programme, grant 614.031.017. Ch.H. is particular gratefully to Vincent Icke and Tim de Zeeuw for the host support during the period of work at the Sterrewacht Leiden. The computer support at the Sterrewacht Leiden and at ESTEC is highly acknowledged. Most of the literature search was done with ADS.

References

Allard, F., Hauschildt, P. H., Alexander, D. R., Tamanai, A., & Schweitzer, A. 2001, ApJ, 556, 357
Ackermann, S., & Marley, M. 2001, ApJ, 556, 872
Anders, E., & Grevesse, N. 1989, Geochem. Cosmochem. Acta, 53, 197
Asplund, M., Grevesse, N., & Sauval, A. J. 2005, in *Cosmic Abundances as Record of Stellar Evolution and Nucleasynthesis*, ed. F. N. Bash, & T. G. Barnes, in press
Bailer-Jones, C. A. L., & Mundt, R. 1999, A&A, 348, 800
Bailer-Jones, C. A. L., & Mundt, R. 2001a, A&A, 374, 1071
Bailer-Jones, C. A. L., & Mundt, R. 2001b, A&A, 367, 218
Burgasser, A. J. 2004, ApJ, 614, L73
Burgasser, A. J., Marley, M. S., Ackermann, A. S., et al. 2002, ApJ, 564, 421
Burgasser, A. J., McElwain, M. W., Kirkpatrick, J. D., et al. 2004, AJ, 129, 2856
Buyevich, Y. A., & Tre'yakov, M. T. 1994, J. Phys. Il France, 4, 1605
Chase Jr., M. W., Davies, C. A., Downey Jr., J. R., et al. 1986, J. Phys. Chem. Ref. Dat., 14(1)
Cooper, C. S., Sudarsky, D., Milsom, J. A., Lunine, J. L., & Burrows, A. 2003, ApJ, 586, 1320
Cowan, J. J., Sneden, C., Burles, S., et al. 2002, ApJ, 572, 861
Cowan, J. J., Sneden, C., Beers, T., et al. 2005, ApJ, 627, 238
Chan, Y. L., Pai, W. W., & Chuang, T. J. 2004, APS, 1200
Chase, Jr., M. W., Davies, C. A., Downey Jr., J. R., et al. 1985, JANAF Thermochemical Tables (National Bureau of Standards)
Chen, D. A., Bartelt, M. C., Hwang, R. Q., & McCarty, K. F. 2000, Surf. Sci., 450, 78
Dominik, C., Sedlmayr, E., & Gail, H. P. 1993, A&A, 277, 578
Geballe, T. R, Knapp, G. R., Leggett, S., et al. 2002, ApJ, 564, 466
Gail, H. P., & Sedlmayr, E. 1984, A&A, 132, 163
Gail, H. P., & Sedlmayr, E. 1986, A&A, 166, 225
Gail, H. P., & Sedlmayr, E. 1988, A&A, 206, 153
Gail, H. P., & Sedlmayr, E. 1998, in The Molecular Astrophysics of Stars and Galaxies, ed. T. W. Hartquist, & D.A. Williams, 285
Gail, H. P., Keller, R., & Sedlmayr, E. 1984, A&A, 133, 320
Hashimoto, A. 1990, Nature, 347, 53
Helling, Ch. 2003, in Rev. Mod. Astro., 16, ed. R. Schielicke (New York, Wiley), 115
Helling, Ch., Oevermann, M., Lüttke, M. J. H., Klein, R., & Sedlmayr, E. 2001, A&A, 376, 194 (Paper I)
Helling, Ch., Woitke, P., Klein, R., & Sedlmayr, E. 2004, A&A, 423, 657 (Paper IV)
Helling, Ch., Thi, W.-F, Woitke, P. & Fridlund, M., 2006, A&A, 451, L9
Jeong, K. S., Chang, C., Sedlmayr, E., & Sülzle, D. 2000, J. Phys. B, 33, 3417
Jeong, K. S., Winters, J. M., Le Bertre, T., & Sedlmayr, E. 2003, A&A, 407, 191
Kirkpatrick, J. D., Reid, I. N., Liebert, J., et al. 1999, ApJ, 519, 802
Korhonen, H., Napari, I., Timmreck, H., et al. 2003, JoGR 108, D17, 4546
Lüttke, M. 2002, Ph.D. Thesis, TU Berlin
Lodders, K., & Fegley, B. Jr. 2005, Astrophysics Update (Springer), submitted
Maiti, M, Sengupta, S., Parihar, P. S., & Anupama, G. C. 2005, ApJ, 619, L183
Martín, E., Zapatero Osorio, M., & Lehto, H. 2001, ApJ, 557, 822
McCarty, K. 2003, APS, 03, 6007
Ménard, F., Delfosse, X., & Monin, J.-L. 2002, A&A, 396, L35
Nagahara, H., & Ozawa, K. 1996, Geochim. et Comsochim. Acta, 60, 1145
Patzer, A. B. C., Gauger, A., & Sedlmayr, E. 1998, A&A, 337, 847
Patzer, A. B. C. 2004, ASPC, 309, 301
Rockenfeller, B., Bailer-Jones, C. A. L., & Mundt, R. 2006, A&A, 448, 1111
Sharp, C. M., & Huebner, W. F. 1900, ApJ, 72, 417
Sedlmayr, E. 1999, in Optical and Infrared Spectroscopy of Circumstellar Matter, ed. Stecklum, Klose, ASPCS, 188, 211
Sengupta, S. 2003, ApJ, 585, L155
Sengupta, S., & Krishan, V. 2001, ApJ, 561, 123
Sengupta, S., & Kwok, S. 2005, ApJ, 625, 996
Stam, D. M., & Hovenier, J. W. 2005 A&A, 444, 275
Stam, D. M., de Haan, J. F., Hovenier, J. W., & Stammes, P. 1999, J. Geophys. Res., 104, 16843
Tsuji, T. 2002, ApJ, 575, 264
Tsuji, T. 2005, ApJ, 621, 1033
Venables, J. A. 1993, Surf. Sci., 299, 798
Woitke, P. 1999, Astronomy with Radioactivities, ed. R. Diehl, & D. Hartmann,, 163
Woitke, P. 2003, IAUS, 210, 387, ed. N. Piskunov, W. W. Weiss, D. F. Gray
Woitke, P., & Helling, Ch. 2003, A&A, 399, 297 (Paper II)
Woitke, P., & Helling, Ch. 2004, A&A, 414, 335 (Paper III)
Zapatero Osorio, M. R., Caballero, J. A., & Béjar, V. J. S. 2005, ApJ, 621, 445

Online Material

Appendix A: Vapour pressure and supersaturation

We consider molecules of kind M_N (the "clusters") which are composed of exactly N units. M_1 is the "monomer". In chemical equilibrium (CE) we can apply the law of mass action to the following hypothetic reaction of type I

$$N \cdot M_1 \leftrightarrow M_N \tag{A.1}$$

to calculate the partial pressures $p^{\rm CE}(N)$ of the clusters

$$\frac{p^{\rm CE}(N)}{p^{\ominus}} = \left(\frac{p^{\rm CE}(1)}{p^{\ominus}}\right)^N \exp\left(-\frac{\Delta_{\rm f}^{\ominus}G(N) - N\Delta_{\rm f}^{\ominus}G(1)}{RT}\right), \tag{A.2}$$

where $p^{\ominus}$ is the standard pressure at which the Gibbs free energy of formation of the N-cluster $\Delta_{\rm f}^{\ominus}G(N)$ and the monomer $\Delta_{\rm f}^{\ominus}G(1)$ have been measured in the laboratory. R is the universal gas constant and T the temperature. Next, we will take Eq. (A.2) to the power of $1/N$ and apply the limit $N \to \infty$. Using the following results for the limiting values

$$\lim_{N\to\infty} \frac{\Delta_{\rm f}^{\ominus}G(N)}{N} = \Delta_{\rm f}^{\ominus}G_{\rm S} \tag{A.3}$$

$$\lim_{N\to\infty} \left(p^{\rm CE}(N)\right)^{1/N} = 1 \tag{A.4}$$

($p^{\rm CE}(N)$ must remain bounded for $N \to \infty$) and identifying the saturation vapour pressure $p_{\rm vap}(T)$ as the partial pressure of the monomer above arbitrarily large clusters (the solid) in phase equilibrium, we find

$$p_{\rm vap}(T) = p^{\ominus} \exp\left(\frac{\Delta_{\rm f}^{\ominus}G_{\rm S} - \Delta_{\rm f}^{\ominus}G(1)}{RT}\right), \tag{A.5}$$

where $\Delta_{\rm f}^{\ominus}G_{\rm S}$ is the Gibbs free energy of formation of a solid unit.

With the thermal equation of state for an N-cluster in chemical equilibrium, $f^{\rm CE}(N) = p^{\rm CE}(N)\,kT$, it follows for sufficiently large clusters which obey $\Delta_{\rm f}^{\ominus}G(N-1) \approx \Delta_{\rm f}^{\ominus}G(N) - \Delta_{\rm f}^{\ominus}G_{\rm S}$

$$\frac{f^{\rm CE}(N-1)}{f^{\rm CE}(N)} = \frac{p^{\rm CE}(N-1)/p^{\ominus}}{p^{\rm CE}(N)/p^{\ominus}} \tag{A.6}$$

$$= \frac{p^{\ominus}}{p^{\rm CE}(1)} \exp\left(\frac{\Delta_{\rm f}^{\ominus}G_{\rm S} - \Delta_{\rm f}^{\ominus}G(1)}{RT}\right) \tag{A.7}$$

$$= \frac{p_{\rm vap}(T)}{p^{\rm CE}(1)(T)}. \tag{A.8}$$

This ratio can be identified with the inverse of the supersaturation ratio in thermal equilibrium ($T \equiv T_{\rm d} \equiv T_{\rm g}$) which is defined as

$$S = \frac{p^{\rm CE}(1)(T)}{p_{\rm vap}(T)}. \tag{A.9}$$

Hence, in phase equilibrium where $S = 1$ and $f^{\rm CE}(N) = \mathring{f}(N)$, we find for large clusters

$$\frac{\mathring{f}(N-1)}{\mathring{f}(N)} = 1. \tag{A.10}$$

In cases where the monomer is not stable as a free molecule (e.g. forsterite Mg_2SiO_4, pyroxene $Mg_{0.7}Fe_{0.3}SiO_3$ etc.), the definition of the supersaturation ratio according to Eq. (A.9) seems to be problematic at first, because S is given by a fraction of two pressures, which are both virtually zero. However, if we consider a fictitious species $M = X_{\rm x}Y_y$ composed of two elements X and Y with stoichiometric coefficients x and y, respectively, the partial pressure of the monomer can be expressed by the respective atomic partial pressures via the law of mass action

$$p^{\rm CE}(1) = p^{\rm CE}_{X_{\rm x}Y_y} = \frac{(p_X^{\rm CE})^x (p_Y^{\rm CE})^y}{(p^{\ominus})^{x+y-1}} \cdot \exp\left(-\frac{\Delta_{\rm f}^{\ominus}G[X_{\rm x}Y_y] - x\Delta_{\rm f}^{\ominus}G[X] - y\Delta_{\rm f}^{\ominus}G[Y]}{RT}\right). \tag{A.11}$$

Inserting Eqs. (A.5) and (A.11) into Eq. (A.9) shows that *the properties of the monomer cancel out*

$$S = \frac{(p_X^{\rm CE})^x (p_Y^{\rm CE})^y}{(p^{\ominus})^{x+y}} \cdot \exp\left(-\frac{\Delta_{\rm f}^{\ominus}G\left[X_{\rm x}Y_y[{\rm s}]\right] - x\Delta_{\rm f}^{\ominus}G[X] - y\Delta_{\rm f}^{\ominus}G[Y]}{RT}\right). \tag{A.12}$$

Thus, the supersaturation ratio S is well-defined, no matter whether the monomer exists in the gas phase or not. Generally speaking, $S > 1$ indicates that it is thermodynamically favourable to convert *any* suitable combination of gaseous species (in chemical equilibrium with each other) into the condensed phase.

Appendix B: Reaction supersaturation ratios

Equation (A.12) states the supersaturation ratio S of the monomer in the gas phase over the respective solid material. Strictly speaking, S equals the ratio between the growth rate and the spontaneous evaporation rate of type I surface reactions in thermal and chemical equilibrium (see Eq. (17)) and in consideration of only one pure solid ($b_{\rm therm} = b_{\rm chem} = b_{\rm surf} = 1$).

However, typical surface reactions for oxygen-rich dust particles are much more complicated, for example

$$2\,{\rm Mg} + {\rm SiO} + 3\,{\rm H_2O} \longleftrightarrow {\rm Mg_2SiO_4[s]} + 3\,{\rm H_2}, \tag{B.1}$$

which we have designated as type III surface reactions. In these reactions, the monomer does not occur and there is in fact no simply way to eliminate the unknown backward reaction rates via the monomer supersaturation ratio S, as it was possible for type I reactions (see Sect. 2.1.2). Instead, we need to introduce a modified reaction supersaturation ratio S_r.

The proper definition of S_r goes as follows. First, we quantify the forward and backward reaction rates per surface area by assuming that these reactions are triggered by the thermally impinging collision rates of two key species (in our example Mg and H_2) with particle densities $n_{f,r}$ and $n_{b,r}$, respectively:

$$\text{forward rate}_r = n_{f,r}^{\rm CE} R_{f,r}(T) \tag{B.2}$$

$$\text{backward rate}_r = n_{b,r}^{\rm CE} R_{b,r}(T). \tag{B.3}$$

For simplicity, we assume chemical equilibrium in the gas phase and thermal equilibrium between gas and dust. The forward reaction rate coefficient $R_{f,r}(T)$ is considered as known, whereas the backward rate coefficient $R_{b,r}(T)$ needs to be eliminated by a suitably defined reaction supersaturation ratio S_r.

Next, we introduce a reference state, designated by $^\circ$, where the gas is in phase equilibrium with the solid s affected by reaction r. This state is characterised by detailed balance where *each* reaction must be balanced exactly by its reverse. Hence, we can write

$$\mathring{n}_{f,r} R_{f,r}(T) = \mathring{n}_{b,r} R_{b,r}(T). \tag{B.4}$$

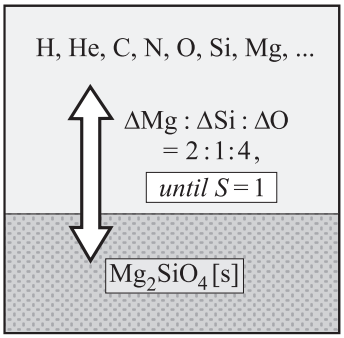

Fig. B.1. Thought experiment to obtain the reference state °.

This is the desired equation to eliminate the unknown backward reaction rate coefficient $R_{b,r}(T)$ and we can deduce

$$\frac{\text{forward rate}_r}{\text{backward rate}_r} = S_r \tag{B.5}$$

with the reaction supersaturation ratio S_r

$$S_r = \frac{n^{\rm CE}_{f,r}}{\mathring{n}_{f,r}} \frac{\mathring{n}_{b,r}}{n^{\rm CE}_{b,r}} = \frac{p^{\rm CE}_{f,r}}{\mathring{p}_{f,r}} \frac{\mathring{p}_{b,r}}{p^{\rm CE}_{b,r}} \tag{B.6}$$

being the suitable analog to the monomer supersaturation ratio S.

The question remains, however, how the reference state is defined precisely. For this purpose, we carry out the following thought experiment as sketched in Fig. B.1. We consider a gas of arbitrary element composition ϵ_k (k = H, He, C, N, O, ...)[9] and bring it in contact with the considered solid s. Now we close the system and wait, giving the system enough time to build up more solid material s from the gas phase or to partially evaporate material s, until an equilibrium is achieved, where all growth reactions are balanced by their reverse, including the (possibly only hypothetical) monomer addition reaction which occurs at $S = 1$. Now we can measure the changed element abundances $\mathring{\epsilon}_k$ and the correspondingly changed partial pressures $\mathring{p}$. Due to stoichiometric constraints, the element abundances in the reference state will satisfy

$$\mathring{\epsilon}_k = \epsilon_k + X \nu^{\rm s}_k \tag{B.7}$$

where X is the number of reactions taken place per H-atom and $\nu^{\rm s}_k$ are the stoichiometric coefficients of element k in solid s. The unknown X can be calculated as the root of $S = 1$ at constant T and $n_{\langle \rm H \rangle}$.

Equations (B.6) and (B.7), with X being the root of $S = 1$, offer a unique way to define the reaction supersaturation ratios S_r for all surface reactions (types I, II or III). The technical disadvantage of this general method, however, is that it requires several calls of the gas phase chemical equilibrium routine as function of X, which itself is a complicated iterative procedure. Therefore, in hydrodynamical applications, the presented method is unacceptably slow and we seek for a further simplification. In any case, we have $S = 1 \Rightarrow S_r = 1$ according to the outlined procedure, consistent with the statements at the end of Appendix A.

The results of the presented general method as function of temperature are shown in Fig. B.2 for the surface reactions listed

[9] This is different from Dominik et al. (1993), who assumed that the element composition of the gas resembles that of the solid, which we think is incorrect.

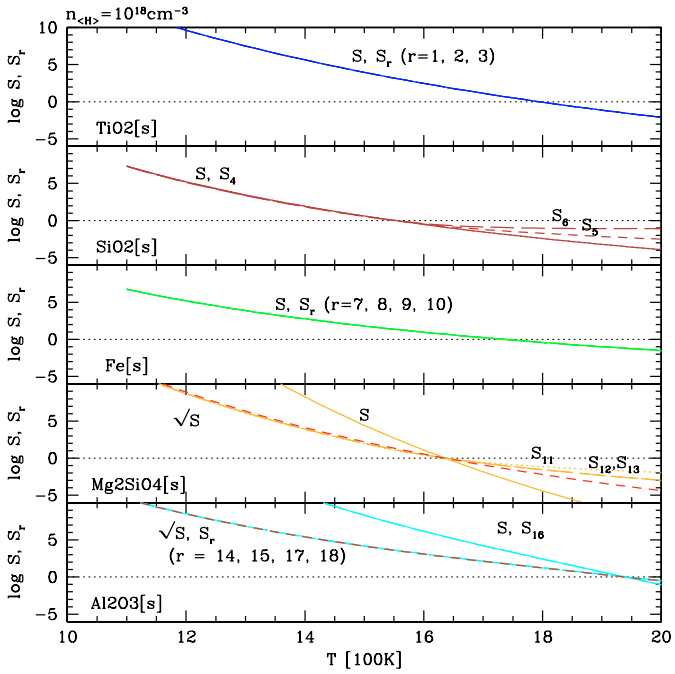

Fig. B.2. Monomer supersaturation ratios S (solid lines) and reaction supersaturation ratios S_r (dashed lines) separately for all considered solids s as function of temperature T at fixed hydrogen nuclei density $n_{\langle \rm H \rangle} = 10^{18}$ cm^{-3}. $\sqrt{S}$ is shown for comparison by the red dashed lines.

in Table 1. For type I surface reactions, the backward rate is spontaneous and a key species for the backward reaction does not exist ($n_{b,r} = 1$). Consequently, we find $\mathring{p}_{f,r} \equiv p_{\rm vap}$ and $S_r \equiv S$ for type I.

None of the reactions in Table 1 is actually of type II. The main difference to type III reactions is that the identification of the key species is trivial since there is simply only one choice for the forward and backward reactions. Considering, for example, the important reaction for the growth of carbonaceous grains $\frac{1}{2}C_2H_2 \leftrightarrow C[s] + \frac{1}{2}H_2$, we have $S_r = \frac{p^{\rm CE}_{\rm C_2H_2}}{\mathring{p}_{\rm C_2H_2}} \frac{\mathring{p}_{\rm H_2}}{p^{\rm CE}_{\rm H_2}}$. Since only carbon is affected by the outlined procedure to reach the reference state, we have $\mathring{p}_{\rm H_2} = p^{\rm CE}_{\rm H_2}$, and since $p^{\rm CE}_{\rm C_2H_2} \propto (p^{\rm CE}_{\rm C})^2$, we find $S_r = (S)^2$. This is exactly the result of Patzer et al. (1998) for this type II reaction in case of thermal and chemical equilibrium.

Concerning the most relevant type III reactions, we find that the following approximation is quite accurate in most cases (compare Fig. B.2):

$$S_r \approx \left(S\right)^{\frac{1}{\nu^{\rm key}_r}} \tag{B.8}$$

where $\nu^{\rm key}_r$ is the stoichiometric factor of the key educt in reaction r. Note that the upper result for the example type II reaction is in accordance with this finding. Turning back to our example type III reaction (Eq. (B.1)), we have

$$S_r = \frac{p^{\rm CE}_{\rm Mg}}{\mathring{p}_{\rm Mg}} \frac{\mathring{p}_{\rm H_2}}{p^{\rm CE}_{\rm H_2}}. \tag{B.9}$$

We take the square of Eq. (B.9) and multiply the nominator and denominator of the result with $\frac{p^{\rm CE}_{\rm Si}\left(p^{\rm CE}_{\rm O}\right)^4}{\mathring{p}^{\rm CE}_{\rm Si}\left(\mathring{p}_{\rm O}\right)^4}$. Using $p_{\rm H_2} = k_f^{\rm H_2}(T)\, p_{\rm H}{}^2$

Table B.1. Monomer volumes $V_{0,s}$ of solid materials from (Lüttke 2002) and fit coefficients c_i for the calculation of the saturation vapour pressures and difference Gibbs free energies. (*): Paper III – (**): Sharp & Huebner (1990).

Condensate	$V_{0,s}$ [10^{-23} cm^3]	c_1	c_2	c_3	c_4	c_5	Fit of	
TiO_2[s]	3.136	35.8027	−74734.7	0.0	0.0	0.0	$\ln p_{\rm sat}$	(*)
SiO_2[s]	3.768	0.0	−4.44364E+5	1.08531E+2	−6.59213E-4	0.0	$\Delta G'$	(**)
Fe[s]	1.178	7.37828E+5	−4.22183E+5	1.71919E+2	−1.76037E-2	2.31459E-6	$\Delta G'$	(**)
Mg_2SiO_4[s]	7.278	7.52334E+4	−9.38369E+5	2.47581E+2	−3.14980E-3	0.0	$\Delta G'$	(**)
Al_2O_3[s]	4.265	0.0	−7.32976E+5	1.84782E+2	−2.57313E-3	0.0	$\Delta G'$	(**)

for both the reference and the chemical equilibrium state ($k_f^{H_2}$ is the equilibrium constant of H_2), we find

$$S_r{}^2 = S \cdot \frac{\mathring{p}_{\rm Si}}{p_{\rm Si}^{\rm CE}} \left(\frac{\mathring{p}_{\rm O}}{p_{\rm O}^{\rm CE}}\right)^4 \left(\frac{\mathring{p}_{\rm H}}{p_{\rm H}^{\rm CE}}\right)^4 . \quad \text{(B.10)}$$

This clarifies why $S_r \approx \sqrt{S}$ is a good approximation for the considered example type III reaction. The required reduction of $\epsilon_{\rm Mg}$ to achieve $S = 1$, which is almost complete for high S (low T), is only connected with a comparably small reduction of $\epsilon_{\rm Si}$, resulting in an almost constant ratio $\mathring{p}_{\rm Si}/p_{\rm Si}^{\rm CE}$ at high S (low T). The changes of $\epsilon_{\rm O}$ and $\epsilon_{\rm H}$ are even less significant such that $\mathring{p}_{\rm H} \approx p_{\rm H}^{\rm CE}$ and $\mathring{p}_{\rm O} \approx p_{\rm O}^{\rm CE}$, hence $S_r \lesssim \sqrt{S}$. Similar arguments can be found for every reaction. The main effect is the reduction of the abundance of the critical element with respect to the stoichiometric ratios of the key educt and the solid, which results in a power of $1/\nu_r^{\rm key}$.

We observe, however, significant deviations from this rule at low S (high T) concerning the solids SiO_2[s] and Mg_2SiO_4[s] (TiO_2[s], Fe[s] and Al_2O_3[s] are OK). For undersaturation, we need to increase the element abundances to achieve $S = 1$. This leads finally to a significant and steady increase of $\mathring{p}_{\rm Si}/p_{\rm Si}^{\rm CE}$ with increasing T, for higher T even for $\mathring{p}_{\rm O}/p_{\rm O}^{\rm CE}$ and $\mathring{p}_{\rm H}/p_{\rm H}^{\rm CE}$. However, these deviations only occur at $S \lesssim 0.1$, which is an extreme value of undersaturation which never occurs in realistic time-dependent models. We want to note, finally, that our theoretical approach favours the evaporation of SiO_2[s] via spontaneous decomposition into monomers (inverse reaction 4) at high T, since $1/S \gg 1/S_5 \gg 1/S_6$ for high T, which is consistent with the experimental results of Hashimoto (1990).

Table C.1. Initial (solar) element abundances from Asplund et al. (2005). All abundances decreased partly considerably compared to Anders & Grevesse (1989).

Element x	Abundance $\epsilon_{\rm x}^0/\epsilon_{\rm H}$
H	1.0
O	4.5709×10^{-4}
N	6.0256×10^{-5}
Al	2.3442×10^{-6}
Si	3.2359×10^{-5}
Mg	3.3884×10^{-5}
Fe	2.8180×10^{-5}
S	1.3804×10^{-5}
Ti	7.9432×10^{-8}
C/O	0.537

Appendix C: Material quantities

The monomer supersaturation ratios are calculated according to Eq. (A.12) where the nominator in the exponential term in Eq. (A.12) is fitted by $\Delta G' = \sum_i c_i T^{i-2}$. The fit coefficients are mostly taken from Sharp & Huebner (1990). Only TiO_2 was treated separately by fitting JANAF table data (electronic version of Chase et al. 1986) with $\ln p_{\rm sat} = \sum_i c_i T^{-i}$ (see Paper III). The coefficients c_i are summarised in Table B.1.